AD_____

Award Number: W81XWH-09-1-0502

TITLE: Breast Cancer-Targeted Nuclear Drug Delivery Overcoming Drug Resistance for Breast Cancer Chemotherapy

PRINCIPAL INVESTIGATOR: Maciej Radosz

CONTRACTING ORGANIZATION: University of Wyoming, Laramie, WY 82071

REPORT DATE: September 2010

TYPE OF REPORT: Annual

PREPARED FOR: U.S. Army Medical Research and Materiel Command
Fort Detrick, Maryland 21702-5012

DISTRIBUTION STATEMENT:

□x Approved for public release; distribution unlimited

REPORT DOCUMENTATION PAGE

Form Approved
OMB No. 0704-0188

1. REPORT DATE *(DD-MM-YYYY)*	**2. REPORT TYPE**	**3. DATES COVERED** *(From - To)*
01-09-2010	Annual	1 SEP 2009 - 31 AUG 2010

4. TITLE AND SUBTITLE
Breast Cancer-Targeted Nuclear Drug Delivery Overcoming Drug Resistance for Breast Cancer Chemotherapy

5a. CONTRACT NUMBER

5b. GRANT NUMBER
W81XWH-09-1-0502

5c. PROGRAM ELEMENT NUMBER

6. AUTHOR(S)
Maciej Radosz, Youqing Shen

5d. PROJECT NUMBER

5e. TASK NUMBER

5f. WORK UNIT NUMBER

7. PERFORMING ORGANIZATION NAME(S) AND ADDRESS(ES)
University of Wyoming
Laramie, WY 82071

8. PERFORMING ORGANIZATION REPORT NUMBER

9. SPONSORING / MONITORING AGENCY NAME(S) AND ADDRESS(ES)
U.S. Army Medical Research and Materiel Command
Fort Detrick, Maryland 21702-5012

10. SPONSOR/MONITOR'S ACRONYM(S)

11. SPONSOR/MONITOR'S REPORT NUMBER(S)

12. DISTRIBUTION / AVAILABILITY STATEMENT
Approved for public release

13. SUPPLEMENTARY NOTES

14. ABSTRACT

Cell membrane-associated and intracellular drug resistance mechanisms are the major cause of breast cancer treatment failure. The ***aim*** of this proposal is to develop nuclear localizing nanoparticles to deliver DNA-toxins breast cancer cell nuclei to effectively overcoming the drug resistance. We finished the task 1— To synthesize and optimize folic-acid– or LHRH-functionalized charge reversal nanoparticles. The cationic polymer PEI and its block copolymer with degradable PCL were synthesized. The cationic PEI block amines were converted to acid labile amides to obtain the PCL-PEI/amide block copolymer. This polymer was used to fabricate the nanoparticles. The ideal nanoparticles with optimal sizes and acid-triggered negative-to-positive charge reversal properties were fabricated and characterized carefully. These nanoparticles will be characterized in vitro and in vivo.

15. SUBJECT TERMS
Nuclear Drug Delivery

16. SECURITY CLASSIFICATION OF: U			**17. LIMITATION OF ABSTRACT**	**18. NUMBER OF PAGES**	**19a. NAME OF RESPONSIBLE PERSON**
a. REPORT	**b. ABSTRACT**	**c. THIS PAGE**	UU	34	USAMRMC
					19b. TELEPHONE NUMBER *(include area code)*

Table of Contents

Page

Introduction…….. 4

Body…….. 5

Key Research Accomplishments……..11

Reportable Outcomes……11

Conclusion……12

References……

Appendices……13

Introduction

We worked according to the TASK 1 in the SOW:

STATEMENT OF WORK

Breast Cancer-Targeted Nuclear Drug Delivery Overcoming Drug Resistance for Breast Cancer Chemotherapy
University of Wyoming, 1000 E Univ Ave, Laramie, Wyoming

MaciejRadosz (PI)
Youqing Shen, Ph.D. (Co-PI)
William J. Murdoch, Ph.D. (Co-PI)

TASK 1. To synthesize and optimize folic-acid– or LHRH-functionalized charge reversal nanoparticles (12 Months):

a. Synthesize linear polyethyleneimine (PEI, Mn ~0.8-10kDa) by ring-opening polymerization.
b. React the PEI with proper 5-membered ring-anhydrides to prepare charge-reversal PEIs (PEI/amides), characterize and optimize their charge-reversal kinetics.
c. Introduce folic acid or LHRH to the PEI/amides using a post-reaction method.
d. Fabricate and characterize TCRNs.
e. Load drugs doxorubicin (DOX), camptothecin (CPT) and other drugs for breast cancer to TCRNs.

Milestone 1: To obtain the FA- and LHRH-functionalized TCRNs with optimal charge-reversal kinetics, targeting group density, size, and drug loading.

TASK 2. To in vitro evaluate the TCRNs for breast cancer chemotherapy (12 Months):

a. In vitro test drug release profile at pH 7.4.
b. Test stability in blood.
c. In vitro test cellular binding (competitive inhibition method).
d. In vitro test cellular uptake of TCRNs (flow cytometry, confocal laser-light scanning fluorescence microscopy).
e. Intracellular trafficking.
f. In vitro cytotoxicity to breast cancer cells.

Milestone 2: To screen out the TCRNs with the highest in vitro anti-breast cancer activity.

TASK 3. To in vivo evaluate TCRNs' anti-breast cancer efficacy (12 months)

a. In vivo test biodistribution and tumor targeting efficiency using nude mice (about 120 mice).
b. In vivo test and compare anticancer activity using nude mice with ip tumors and sc tumors treated by ip and iv injections (about 200 mice).

Milestone 3: To screen out the TCRNs with the highest in vivo anticancer activity

Body

1. Charge-Reversal Linear Polyethyleneimine-Based Nanoparticles for Nuclear-Targeted Drug Delivery

Experimental

Materials: 2,3-dimethylmaleic anhydride (DM) (98%), *N,N'*-Dicyclohexylcarbodiimide (DCC), *N*-hydroxysuccinimide (NHS), 2-methyl-2-oxazoline (MeO_Z, 98%) and methyl p-toluenesulfonate (MeOTs) were purchased from Sigma-Aldrich and used as received. ε-Caprolactone (ε-CL) (Aldrich) was dried over calcium hydride. 1,2-Distearoyl-sn-glycero-3-phosphoethanolamine-*N*-((Polyethylene glycol-2000) folate) (ammonium salt) (DSPE-PEG-Folate) was purchased from Avanti polar lipids INC. PCL with a molecular weight of 2000 terminated with an NHS active ester (PCL_{18}-NHS) was synthesized as we previously reported.

Preparation of LPEI terminated with an primary amine (LPEI-NH_2):

LPEI-NH_2 with different molecular weights was synthesized by cationic ring-opening polymerization of 2-methyl-2-oxazoling (MeO_Z). Methyl p-toluenesulfonate (MeOTs) (0.484 g, 2.6 mmol)was added to the MeO_Z (10 mL, 117 mmol) in acetonitrile (50 mL). The solution was stirred at 75 ^oC for 3 days. The polymerization was terminated by adding ethylenediamine (2 mL, 30 mmol) at 40 ^oC for 24 h. The polymer was precipitated in cold diethyl ether (500 mL). A white powder was obtained after drying in vacuum with a yield of 91%. The molecular weight of the $PMeO_Z$ was determined by ^1H NMR and gel permeation chromatography (GPC) using polystyrene standards. PMeOz ^1H NMR (400 MHz, $CDCl_3$, δ): 2.1 (3H, $COCH_3$), 2.6 (ethylenediamine end group, $NHCH_2CH_2NH_2$), 3.5 (4H, NCH_2CH_2). PMeOz (3 g) was refluxed in hydrochloric acid (85 mL, concentration: 13%) at 110 ^oC for 24 h. A white solid was precipitated out, filtered and dried to obtain LPEI hydrochloride salt. The polymer was dissolved deionized water, and the solution pH was adjusted to 8.2 using 3 M KOH. The solution was dialyzed against DI water (MWCO=1,000, 1L×3) and freeze dried to obtain LPEI with a yield of 48%. The molecular weight of the PEI was also determined by MALDI-TOF. LPEI ^1H NMR (400 MHz, D_2O, δ): 2.8 ppm (4H, $NHCH_2CH_2$).

Preparation of PCL_{18}-$LPEI_{23}$, PCL_{18}-$LPEI_{35}$, PCL_{18}-$LPEI_{46}$ block copolymers: PCL_{18}-NHS (0.5 g, 0.25 mmol) was dissolved in 30 mL methanol and $LPEI_{23}$-NH_2 (0.30 mmol) (or $LPEI_{35}$-NH_2, or $LPEI_{46}$-NH_2) in 10 mL methanol was then added to the solution. The mixture was kept at 60 ^oC for 12 h. After cooling to room temperature, the solution was poured into cold diethyl ether and the solid was isolated. The crude product was then dispersed in DI water and dialyzed against DI water to remove free LPEI (pH 7.4, MWCO=10,000, 2L×3). The solution was then freeze dried to obtain the block copolymer at a yield of 75%. ^1H NMR of PCL_{18}-$LPEI_{23}$ (400 MHz, DMSO-d6, δ, ppm): 0.84 (end group of PCL, CH_3), 1.24 (2H, $CH_2CH_2CH_2$), 1.55 (4H, $CH_2CH_2CH_2$), 2.27 (2H, CH_2CO), 2.74 (4H, NCH_2CH_2), 4.06 (2H, OCH_2). Other block copolymers were prepared similarly.

Preparation of PCL-LPEI/DM: PCL-LPEI was dispersed into DI water with ultrasound and the solution pH was adjusted to 8.5. DM (10 times (molar) of the NH group in LPEI) was added by portions and the pH was maintained at 8.5 by adding 1 M NaOH. The solution was kept stirring for 30 min after all the DM was added. The solution was then dialyzed against water (pH 8.5, MWCO=1,000, 2L×3) followed by freezing dried. The degree of amidization was determined by ^1H NMR. ^1H NMR of PCL-LPEI/DM (400 MHz, D_2O, δ in ppm): 1.25 (2H, $CH_2CH_2CH_2$), 1.50 (4H, $CH_2CH_2CH_2$), 1.72 (6H, CH_3), 2.17 (2H, CH_2CO), 2.64 (4H, NCH_2CH_2), 3.33 (4H, $CONCH_2CH_2$), 3.91 (2H, OCH_2).

Fabrication of the folate receptor-targeted DOX-loaded charge-reversal nanoparticles PCL-FLPEI/DM-DOX: DSPE-PEG-Folic acid (0.2 mg) was mixed with PCL_{18}-$LPEI_{48}$/$DM_{60\%}$ (2 mg) in methanol (1 mL) and acetone (0.5 mL) mixed solvent. DOX·HCl (0.5 mg) and triethylamine (5 μL) were

dissolved in DMSO (1 mL). The two solutions were mixed and stirred at room temperature for 1 h. The solution was dialyzed against DI water (pH 8.5, 2L×3) and then transferred to a centricon centrifugal filter device (YM-3, 10,000 MWCO, Millipore Corp., Bedford, MA) to remove free DOX. The DOX loading was analyzed by measuring its UV absorbance at 486 nm in DMSO/methanol. The encapsulation efficiency was 78% and the loading content was 14.3%.

MALDI-TOF spectra: α-cyano-4-hydroxycinnamic acid was used as the matrix for MALDI-TOF measurements. The matrix was prepared at a concentration of 10 mg/mL in THF. The sample solution (1 μL) was applied to the MALDI sample plate and dried. The matrix solution (1 μL) was then added to the plate and dried. The instrument was operated in a linear mode. A N_2 laser radiating at 337 nm with 3 ns pulses was used. The ions generated by the laser pulses were accelerated to 20 kV.

Size and Zeta-potential measurements: The sizes (diameter) of PCL-LPEI, PCL-LPEI/DM and PCL-FLEPI/DM/DOX nanoparticles were determined using a Nano-ZS zetasizer (Malvern Instrument Ltd., UK) with a laser light wavelength of 632.8 nm and a scattering angle at 173°. The nanoparticles were prepared as described above. The zetasizer was routinely calibrated with a 60 nm nanosphere™ standard (Duke Scientific Corp. CA). Each measurement was performed in triplicate, and the results were processed with DTS software version 3.32.

Zeta-potential measurements: The ζ-potentials of the nanoparticles were measured using phase-analysis light-scattering technology. PCL-LPEI/DM was dispersed in a PBS (0.1 M) at pH of 7.4, 6.0, or 5.0 at 1 mg/mL. The solution was transferred to a dialysis bag and dialyzed in the same PBS at 37 ^oC with shaking. Samples were taken at timed intervals and their ζ-potentials were measured using the Zeta-Nanosizer, which was routinely calibrated with a -50 mv zeta-potential standard (Malvern Instruments). The attenuator was set at 9 and the F (Ka) value was set at 1.5. Each measurement was performed for 30 runs, and the results were processed with DTS software version 3.32.

Critical micelle concentration (CMC) determination: CMC of the polymers was determined using our reported method: A stock solution of the copolymer (2 mg/mL) was prepared in 10 mM pH 7.4 phosphate buffer. Nile red in CH_2Cl_2 (10 μL, 0.5 mg/mL) was added to a series of vials and the CH_2Cl_2 was evaporated. The copolymer solution and 10 mM pH 7.4 phosphate buffer were added to vials to obtain the polymer concentrations ranging from 0.0039 to 2 mg/mL. The vials were then stirred at room temperature overnight. The fluorescence emission of the solution was measured. The CMC was determined as the intersection of the tangents to the two linear portions of the plot of the emission intensity as a function of the polymer concentration.

Transmission Electron Microscopy (TEM) of the Nanoparticles: The nanoparticles solution (2 mg/mL, 10 μl) was applied onto a 150-mesh carbon-coated copper grid. The excess solution was wicked off with filter paper. This coating procedure was repeated twice. Images were recorded using a transmission electron microscope (HITACHI H-7000 TEM) operated at a voltage of 75 kV with an original magnification of 20,000.

Amide hydrolysis Studied by ^1H NMR Spectroscopy: The hydrolysis of β-carboxylic acid amide in PCL-LPEI/DM was monitored by ^1H NMR spectroscopy as follows. PCL-LPEI/DM was dispersed in PBS (10 mmol, pH at 11, 7.4, 6.0 or 5.0). The solution was loaded to a dialysis bag (MWCO=1,000) and dialyzed against PBS at the same pH at 37 ^oC with shaking. At timed interval, samples were withdrawn from the dialysis bag and the solution pH was adjusted to 11.0. The samples were freeze dried and then dissolved in D_2O. The solution pH was maintained at 11.0 using a D_2O solution of DOH or DCl to separate the signal of the ethylene with amino group ($NHCH_2$) from that with amide group ($C(O)NCH_2$) in the NMR spectra. The ^1H NMR spectra were recorded on a Bruker Avance DRX-400 spectrometer.

Hemolysis assay: The lysosomal membrane disruption activity of the polymers was measured using a red blood cell (RBC) hemolysis assay. Sheep RBC stock solution was prepared as we previously reported. PCL_{18}-$LPEI_{23}$/$DM_{60\%}$ was prehydrolyzed at pH 6.0 for 0, 12 or 24 h, respectively. The polymers

were collected. Each of them was dispersed in PBS at pH 7.4 at concentrations of 0.01, 0.05, 0.1 and 0.4 mg/mL, respectively. The polymer solution (100 µL), gelatin/veronal buffer (GVB, 200 µL), and RBC stock solution (100 µL) were added to a tube. The tube was incubated at 37 ^{o}C for 2 h, and then 2 mL of 0.15 M NaCl was added to the tube. The tube was centrifuged (1000 g, 3 min) to separate the intact RBCs. The supernatant solution was collected. Absorbance of hemoglobin in the supernatant was measured at 412 nm using a UV-vis spectrophotometer. The observed hemolysis of RBC in PBS (pH 7.4) and in Milli-Q water were used as negative and positive controls, respectively. The observed hemolytic activity of a given polymer at a given concentration was normalized to that of the positive control. All hemolysis experiments were carried out in triplicate.

Cell culture: MCF 7 breast cancer and SKOV-3 adenoccarinoma cells were purchased from American Type Culture Collection (Rockville, MD). Cells were cultured in RPMI-1640 medium containing 10% fetal bovine serum (FBS), 10 µg/mL insulin, and 1% antibiotic/antimycotic solution (Sigma A9909) at 37 ^{o}C in a 5% CO_2 environment. The cells used for cellular uptake and in-vitro cytotoxicity assay of the FA-functionalized nanoparticles were cultured in folic-free medium (Invitrogen Corp.) for at least two weeks before use.

Cellular uptake and intracellular colocalization of the nanoparticle: Cellular uptake and intracellular colocalization of the nanoparticle were observed using confocal fluorescence microscopy. For the colocalization of nanoparticles in lysosomes, cells were incubated with nanoparticle solution at 2 µg/mL DOX at 37 ^{o}C and 5% CO_2 for 4 h. LysoTracker green DND-99 (Molecular Probes, Eugene, OR) (150×10^{-9} M) was then added and the cells were incubated for 2 h. The cells were then thoroughly washed with PBS at 4 ^{o}C three times. For the nuclear localization of the nanoparticles, the cells were incubated with nanoparticles containing 4 µg/mL DOX at 37 ^{o}C and 5% CO_2 for 10 h. DRAQ 5 nuclei dye (1 µL) (Biostatus, 5×10^{-3} M) was added just before the observation. Images were obtained using a Leica TCS SP2 microscope. DOX was observed using Ar/ArKr 458/488 nm laser and the emission wavelength was read from 560 to 610 nm and expressed as red. LysoTracker was observed using Ar/ArKr 458/488 nm laser and the emission wavelength was read from 510 to 540 nm and expressed as green. DRAQ 5 nuclei dye was observed using a HeNe 633 nm laser and emission wavelength was read from 660 to 760 nm and expressed as blue. Images were produced by using the lasers sequentially with a 63 × objective lens. Cells were kept at 37 °C and 5% CO_2 except when being observed on the microscope. Images were processed with NIH ImageJ.

In vitro cytoxicity assay: The cytotoxicity assay was carried out using the MTT cell proliferation assay kit (ATCC, Manassas, VA) according to the modified manufacturer's protocol. SKOV-3 cells were cultured in folic-free medium (Invitrogen Corp., Carlsbad, CA) for at least two weeks before use. They were then seeded onto 96-well plates and incubated for 24 h. The original medium (200 µL) was removed and replaced with the PCL-FLEPI/DM/DOX or free DOX solutions at different concentrations and incubated for 24 h or 48 h. The medium in each well was then replaced with fresh cell culture medium and further incubated for 24 h. MTT reagent (10 µL) was then added to each well and incubated for 6 h until purple precipitates were visible. Finally, the detergent reagent (100 µL) was added to each well, and the plates were incubated at 37 ^{o}C for 18 h until all the crystals were dissolved. The absorbance intensity at 570 nm was recorded and the cytoxocity was expressed as a percentage of the control.

Results and Discussion

Design and Synthesis of the Targeted Nuclear-Localizing Drug-Carrier

The nanoparticles with a negative-to-positive charge-reversal linear PEI shell triggered by the lysosomal pH (4-5) for nuclear drug delivery was designed as show in Scheme 1. The secondary amines in linear PEI block were partially amidized to acid-labile amides to inhibit its interactions with cells before reaching tumor tissues, but once at the acidic lysosomes (pH 4-5), the amides quickly hydrolyzed

to regenerate the LPEI. PEI is known to be able to rupture lysosomes via “proton-sponge” effect. Thus, the regenerated PEI can help the nanoparticles to escape from the lysosomes into cytosol, and further lead them to localize in the nucleus. The negatively charged nanoparticles generally have low cellular uptake due to electrostatic repulsion with the cells. Many cancer cells including SKOV-3 ovarian cancer cells overexpress folate receptors. The folic targeting groups were thus introduced to the surface of the nanoparticles using the DSPE-PEG-folate, for receptor-mediated endocytosis. A DNA-toxin DOX was loaded into the nanoparticles.

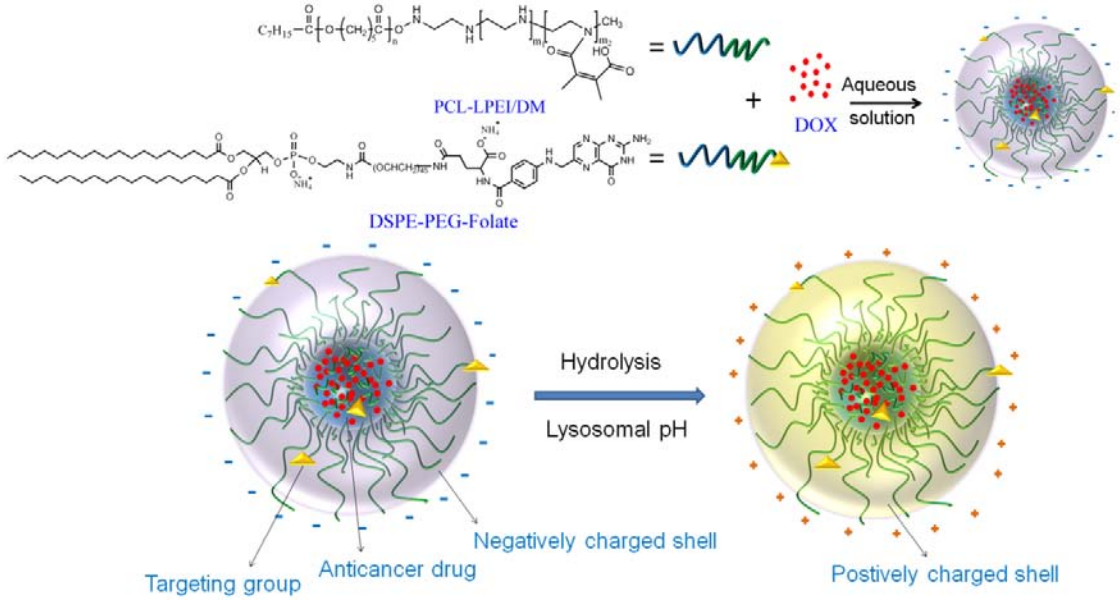

Scheme 1. The sketch of fabrication of the folate targeted charge reversal nanoparticle (TCRN) and its charge-reversal at lysosomal pH.

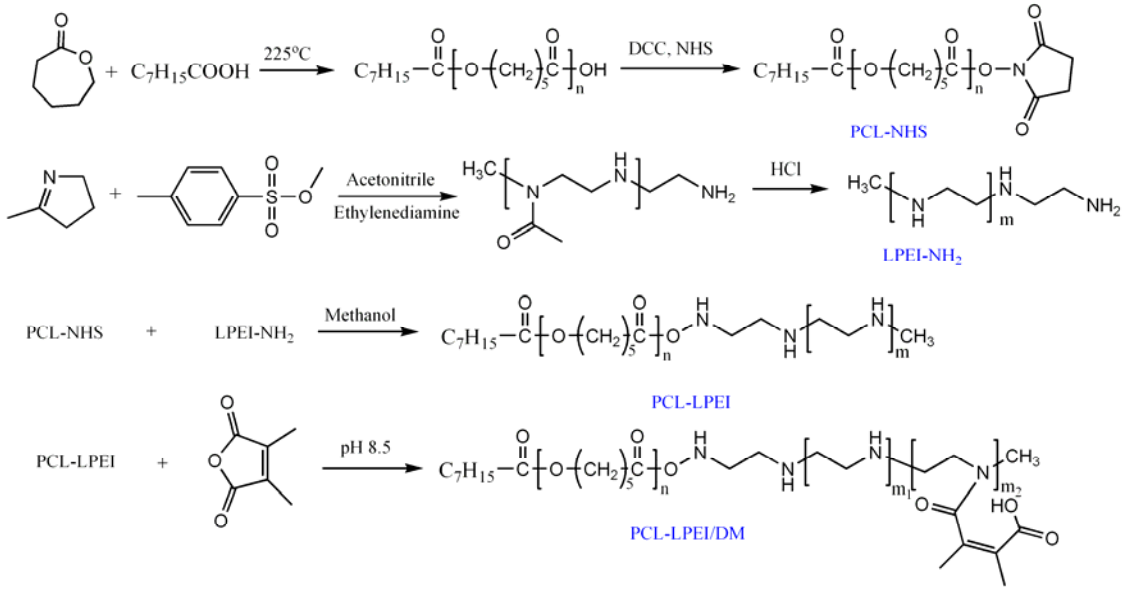

Scheme 2. The synthesis of PCL-LPEI/DM.

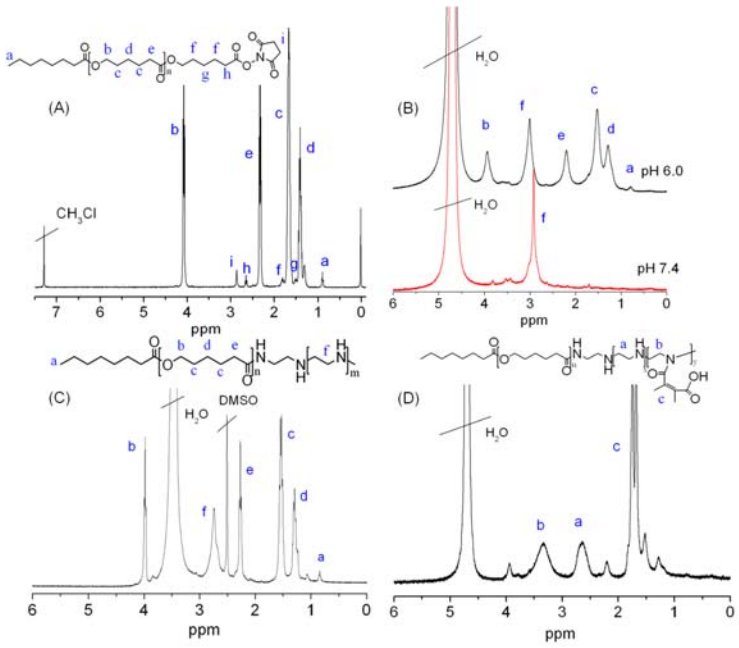

Figure 1. The ^{1}HNMR spectra of PCL-NHS (A), PCL_{18}-$LPEI_{23}$ in D_2O at pH 6.0 and 7.4 (B), PCL_{18}-$LPEI_{23}$ in DMSO-d_6 (C) and PCL_{18}-$LPEI_{23}$/$DM_{60\%}$ in D_2O (D).

The synthesis of the PCL-LPEI/DM is shown in Scheme 2. PCL was synthesized by ring-opening polymerization of ε-CL initiated by octanoic acid and its carboxyl end group was converted to active *N*-hydroxysuccinimide ester (PCL-NHS). The PCL-NHS had repeat units of 18 (molecular weight of 2000) as characterized by ^{1}H NMR (Fig. 1 A). LPEI was prepared by ring-opening polymerization of MeO_Z at different monomer/initiator (MeO_Z/MeOTs) ratios followed by hydrolysis in hydrochloride solution. Three LPEI samples with molecular weights of about 1.0KDa, 1.5KDa and 2.0KDa determined by MALDI-TOF were prepared. A terminal primary amine was introduced to the linear PEI by terminating the reaction with ethylenediamine. An excess of LPEI-NH_2 was then reacted with PCL-NHS to prepare the block polymer PCL-b-LPEI. After the excess free LPEI was removed by dialysis, pure PCL-b-LPEI was obtained, as confirmed by ^{1}H NMR (Fig. 1 B and C) and MALDI-TOF (Fig. 2). At pH 6 protonation of the PEI block solublizes the block copolymers and thus the signals of PCL were also present in the NMR spectra; but at pH7.4 the PCL signals disappeared, indicating that the block copolymer formed micelles with PCL in the core because the PEI solubility decreased. The size of PCL-LPEI formed nanoparticles in aqueous determined by dynamic laser light scattering is shown in Figure 3. PCL_{18}-LPEI with LPEI of 1000 (DP = 23), 1500 (DP = 34) or 2000 (DP = 46) formed nanoparticles with average diameters of 90, 136 and 172 nm, respectively. PCL_{18}-$LPEI_{23}$ nanoparticles were less than 100 nm and thus selected for further characterizations.

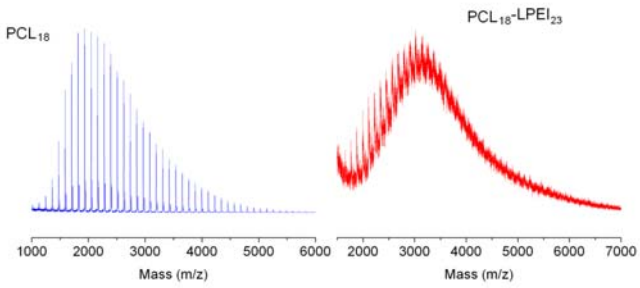

Figure 2. The MALDI-TOF of PCL_{18} and PCL_{18}-$LPEI_{23}$.

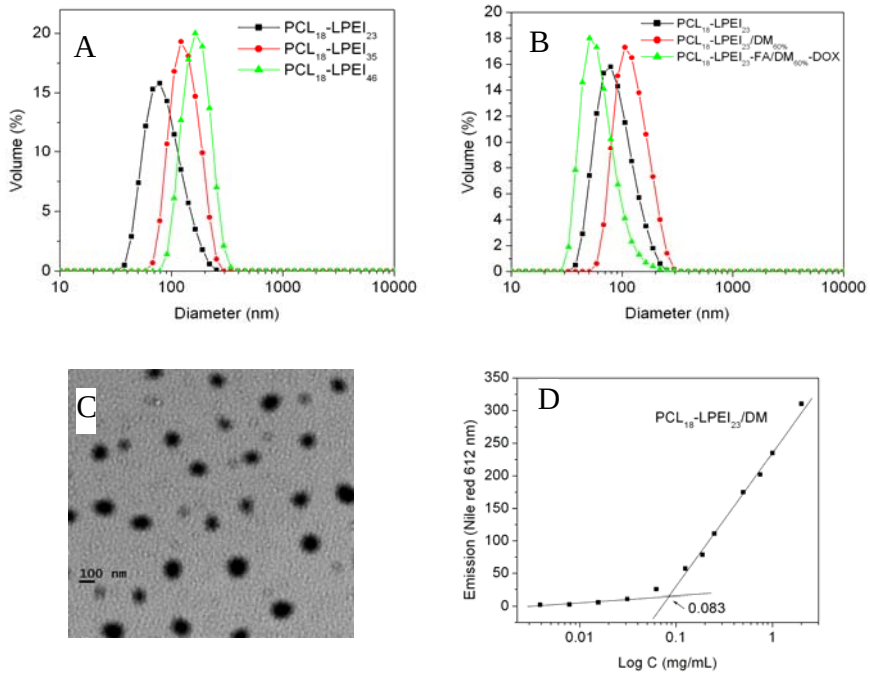

Figure 3. The size of PCL_{18}-$LPEI_{23}$, PCL_{18}-$LPEI_{35}$, PCL_{18}-$LPEI_{46}$ (A) and PCL_{18}-$LPEI_{23}$, PCL_{18}-$LPEI_{23}/DM_{60\%}$, PCL_{18}-$LPEI_{23}$-$FA/DM_{60\%}$-DOX (B), the TEM image of PCL_{18}-$LPEI_{23}$-FA/DM-DOX (C), and the CMC of PCL_{18}-$LPEI_{23}$/DM (D).

The second amine groups on the LPEI block was then reacted with DM anhydride at pH 8.5 and the degree of amodization was determined by ^{1}H-NMR. The signals of methylene protons of -C*H*$_2$NH- and its amide (—CH$_2$—N(—)—C(=O)—) are overlapped in the ^{1}H NMR spectrum at the neutral or lower pH, but the two peaks were well separated, at 2.64 and 3.33 ppm, at pH 11 or higher (Fig. 1 D). By calculating their integrations, the amidization degree was found 60%. The micelle size increased slightly from 96 to 112 nm after the LPEI block was amidized (Fig.3 B). The critic micelle concentration was determined to be 83 mg/L (Fig.3 D).

The pH-triggered hydrolysis and charge reversal

The nanoparticles are expected to be negatively charged at physiological pH (pH 7.4) to inhibit their nonspecific interaction with cells, but should quickly hydrolyze to regenerate cationic LPEI at the tumor extracellular pH (pH<7) or the endosomal/lysosomal pH (pH 4-5) for cellular uptake, endosomal/lysosomal escape, and nuclear localization. For primary amine, its β-carboxylic acid amide from DM hydrolyzed too quickly even at the neutral pH, and the amide from DCA was found optimal in terms of the stability at the neutral pH and rate of hydrolysis at acidic pH. We did the same optimization and found that for the secondary amine in LPEI, the amide from DM was optimal, as shown in Figure 4A. The amide was very stable at pH 11, hydrolyzed very slowly at pH 7.4 but quickly at acidic pH. The times needed for 50% of the amide to hydrolyze were 3.0 h at pH 5.0 and 7.7 h at pH 6.0. At pH 7.4, the amide only hydrolyzed about 30% even after 40 h.

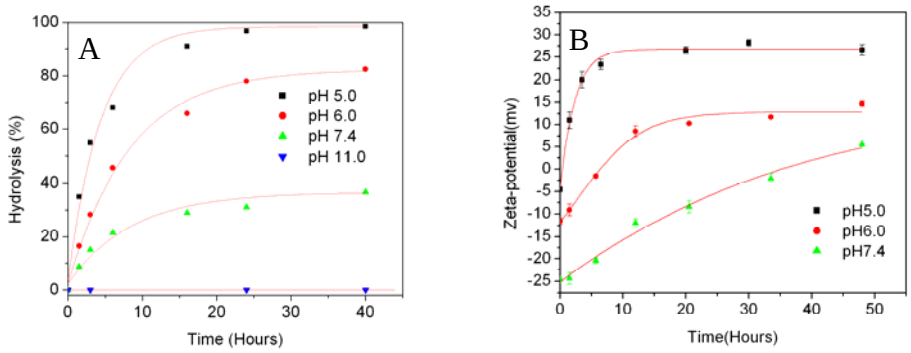

Figure 4. (A) The Hydrolysis of PCL_{18}-$LPEI_{23}$/$DM_{60\%}$ at pH 5.0, 6.0, 7.4 and11.0 in PBS 0.1M at 37 ^{o}C, detected by ^{1}H NMR; (B) the zeta-potential of PCL_{18}-$LPEI_{23}$/$DM_{60\%}$ at pH 5.0, 6.0 and 7.4 as a function of time.

Accordingly, the ζ-potentials of the PCL-LPEI/DM as a function of time at different pH values are shown in Figure 4B. PCL-LPEI/DM had ζ-potentials of about -25 mV, -12 mV and -5 mV at pH 7.4, 6.0 and 5.0, respectively. At pH 7.4, the zeta-potential gradually increased with time but remained negatively charged even after 40 h. At pH 6.0 and 5.0, the time for it to become positively charged (ζ-potential higher than zero) was 6.5 and 0.4 h. These trends are consistent with the hydrolysis results in Figure 4, suggesting that the hydrolysis of the amide induced the negative-to-positive charge reversal.

Key Research Accomplishments

1. We synthesized cancer cell-targeted charge-reversal drug-loaded nanoparticles for nuclear drug delivery to enhance the drug's cytotoxicity. Linear PEI's positive charges are masked by converting them into latent amides, which significantly inhibits its ability to interact with cells.

2. Use curcumin to potentiate breast cancer treatment: Curcumin is a natural herb having low toxicity but has been shown having in vitro anti-breast cancer activity. While working on the nuclear localizing nanoparticles proposed in this project, we also test possibility using curcumin as drug carriers to deliver drugs to have synergetic therapeutic effect. This work is published in two papers. Appendix 1 and 2.

Reportable Outcomes:

Publications

1. Zhou, Z; Shen, Y; Tang, J; Fan, M; Van Kirk, E A.; Murdoch, WJ.; Radosz, M. **Charge-Reversal PEI-nanoparticles for Cascade Nuclear Drug Delivery.** submitted.
2. Tang HD, Murphy CJ, Zhang B, Shen YQ, Van Kirk EA, Murdoch WJ, et al. Curcumin polymers as anticancer conjugates. Biomaterials 2010 Sep;31(27):7139-7149.
3. Tang HD, Murphy CJ, Zhang B, Shen YQ, Sui MH, Van Kirk EA, et al. Amphiphilic curcumin conjugate-forming nanoparticles as anticancer prodrug and drug carriers: in vitro and in vivo effects. Nanomedicine-Uk 2010 Aug;5(6):855-865.
4. Shen YQ, Jin EL, Zhang B, Murphy CJ, Sui MH, Zhao J, et al. Prodrugs Forming High Drug Loading Multifunctional Nanocapsules for Intracellular Cancer Drug Delivery. J Am Chem Soc 2010 Mar 31;132(12):4259-4265.

Era of Hope 2011:

TARGETED CHARGE-REVERSAL DRUG CARRIERS FOR NUCLEAR DRUG DELIVERY FOR BREAST CANCER CHEMOTHERAPY

Youqing Shen, Maciej Radosz and William J. Murdoch

Abstract

Most cancer chemotherapy drugs target nuclear DNA to cause DNA damages and/or topoisomerase inhibition to induce cell death (apoptosis). In addition to the membrane-associated multidrug resistance, drug-resistant cancer cells also have many intracellular drug-resistance mechanisms to limit the access of drugs to the nucleus. Consequently, only a small percentage of drugs delivered into the cytosol finally reach the nucleus in drug-resistant cells. Thus, a drug carrier capable of localizing and releasing drugs directly into the nucleus would circumvent both the multidrug resistance and intracellular drug resistance mechanisms, leading to a high therapeutic efficacy.

Cationic polymers such as polyethyleneimine (PEI) and polylysine (PLL) can carry DNA across the cell membrane and harness the molecular motors to enter the nucleus. However, PEI and PLL have a rapid plasma clearance due to their positive charges from their amine groups.

An ideal regime would be to activate the cationic charges only in cancerous tissues or their intracellular compartments. Herein, we report drug carriers with a negative-to-positive charge reversal triggered by the solid tumor extracellular (pH <7) or lysosomal (4-5) acidity for nuclear drug delivery. The carriers are negatively charged in the bloodstream and have long circulation times. The drugs loaded in the charge-reversal carriers have a higher cytotoxicity than free drugs.

This work was supported by the U.S. Army Medical Research and Materiel Command under W81XWH-09-1-0502.

Conclusion:

We finished the task 1— To synthesize and optimize folic-acid– or LHRH-functionalized charge reversal nanoparticles. The cationic polymer PEI and its block copolymer with degradable PCL were synthesized. The cationic PEI block amines were converted to acid labile amides to obtain the PCL-PEI/amide block copolymer. This polymer was used to fabricate the nanoparticles. The ideal nanoparticles with optimal sizes and acid-triggered negative-to-positive charge reversal properties were fabricated and characterized carefully. These nanoparticles will be characterized in vitro and in vivo.

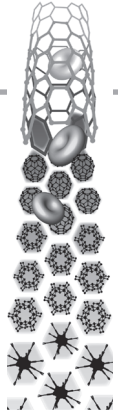

Appendix 1

Amphiphilic curcumin conjugate-forming nanoparticles as anticancer prodrug and drug carriers: *in vitro* and *in vivo* effects

Curcumin has been shown to have high cytotoxicity towards various cancer cell lines, but its water insolubility and instability make its bioavailability exceedingly low and, thus, it is generally inactive in *in vivo* anticancer tests. Here, we report an intracellular-labile amphiphilic surfactant-like curcumin prodrug – curcumin conjugated with two short oligo(ethylene glycol) (Curc-OEG) chains via β-thioester bonds that are labile in the presence of intracellular glutathione and esterase. Curc-OEG formed stable nanoparticles in aqueous conditions and served two roles – as an anticancer prodrug and a drug carrier. As an anticancer prodrug, the formed nanoparticles had a high and fixed curcumin-loading content of 25.3 wt%, and released active curcumin in the intracellular environment. Curc-OEG had high inhibition ability to several cancer cell lines due to apoptosis. Intravenously injected Curc-OEG significantly reduced the tumor weights and tumor numbers in the athymic mice xenografted with intraperitoneal SKOV-3 tumors and subcutaneous (mammary fat pad) MDA-MB-468 tumors. Preliminary systemic toxicity studies found that Curc-OEG did not cause acute and subchronic toxicities to mouse visceral organs at high doses. As drug carriers, Curc-OEG nanoparticles could carry other anticancer drugs, such as doxorubicin and camptothecin, and ship them into drug-resistant cells, greatly enhancing the cytotoxicity of the loaded drug. Thus, Curc-OEG is a promising prototype that merits further study for cancer therapy.

KEYWORDS: anticancer ■ curcumin ■ drug carrier ■ nanoparticle

Huadong Tang[2*], Caitlin J Murphy[3*], Bo Zhang[2], Youqing Shen[†1,2], Meihua Sui[1], Edward Alva Van Kirk[3], Xiaowen Feng[4] & William J Murdoch[3*]

[1]Center for Bionanoengineering & the State Key Laboratory for Chemical Engineering, Department of Chemical & Biological Engineering, Zhejiang University, Hangzhou, 310027, China
[2]Department of Chemical & Petroleum Engineering, University of Wyoming, Laramie, WY 82071, USA
[3]Department of Animal Science, University of Wyoming, Laramie, WY, 82071, USA
[4]The First Affiliated Hospital, School of Medicine, Zhejiang University, Hangzhou, 310027, China
[†]Author for correspondence:
Tel.: +86 571 8795 3993
Fax: +86 571 8795 3993
shenyq@zju.edu.cn
**Authors contributed equally*

Curcumin, a naturally abundant polyphenol, has a wide range of therapeutic activities [1–3], particularly its antitumor properties [4]. Curcumin was found to interact with a wide variety of cell signaling proteins [2,5–7] and downregulate multidrug resistance (MDR) proteins [8,9]. Thus, curcumin has been shown to inhibit the proliferation of a wide variety of cancer cell lines *in vitro* [4,10–14] and *in vivo* tumor growth [15–18] and invasion [19–21], and potentiate radiotherapy [22,23] and chemotherapy [24,25]. Most attractively, curcumin has been clinically proven to have no systemic toxicity to human visceral organs even at very high doses [26–28]. It was also shown to be harmless to normal mouse brain cells [17].

Unfortunately, curcumin is generally found inactive in clinical trials, primarily due to its water insolubility and instability, and thus exceedingly poor bioavailability [28,29]. Curcumin is hydrophobic and practically insoluble in water at acidic conditions; while it quickly degrades in neutral and alkaline conditions with a half-life ($t_{1/2}$) of less than 10 min in phosphate buffered saline (PBS) at pH 7.2 [30], resulting in extremely low bioavailability in both vascular and oral administration. For example, in patients orally administrated up to 3.6 g curcumin, only low nanomolar levels of curcumin were detected in their peripheral or portal circulation [27].

While an ongoing effort is to search stable curcumin analogs [31,32], curcumin delivery by nanocarriers has recently been explored to overcome these limitations. Curcumin loaded in liposomes [10,13,33–35], nanoparticles [36] or conjugated to dendrimers [37] had improved water solubility, stability and, thus, bioavailability. These systems, however, had disadvantages, such as low loading efficiency and loading contents, varied loading contents from batch to batch. Curcumin was also conjugated to polyethylene glycol (PEG) through a liable urethane linkage to prepare water-soluble curcumin derivatives, but they were not stable and readily hydrolyzed even at the neutral conditions (PBS; pH 7.4; $t_{1/2}$ = 60 and 200 min, respectively) [38]. Even though the conjugates showed *in vitro* cytotoxicity against PC-3 pancreatic carcinoma cells, so far no *in vivo* results were presented or followed this research.

Taking advantage of the strong hydrophobicity of the curcumin molecule, in this work we designed an amphiphilic curcumin-based surfactant-like molecule by introducing two short hydrophilic ethylene glycol oligomer (OEG) chains to curcumin (Curc-OEG; Figure 1A). The Curc-OEG formed stable micelles (nanoparticles) in aqueous conditions and had two roles. As a prodrug, the nanoparticles had a fixed and high

part of future medicine fsg

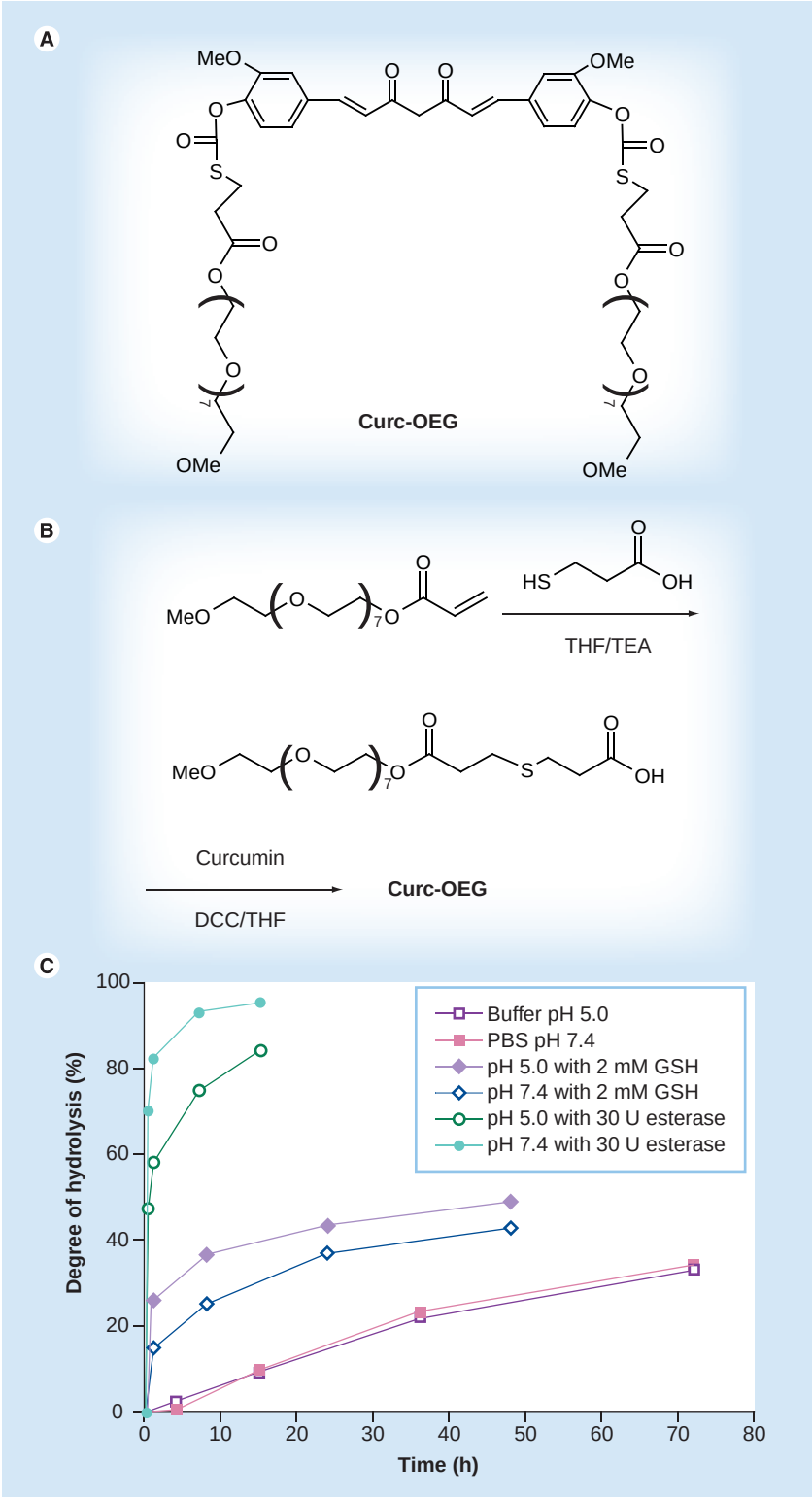

Figure 1. (A) Amphiphilic curcumin conjugated with two oligo(ethylene glycol) chains, (B) its synthetic route and (C) its hydrolysis kinetics.
Curc-OEG: Curcumin conjugated with two oligo(ethylene glycol) chains; DCC: Dicyclohexylcarbodiimide; GSH: Glutathione; PBS: Phosphate buffered saline; TEA: Triethylamine; THF: Tetrahydrofuran.

curcumin-loading content (25.3 wt%), and may target tumors via passive accumulation through the enhanced permeability and retention effect of tumors [39]; once in the intracellular environment the nanoparticles released active curcumin exhibiting very high bioavailability, enhanced *in vitro* cytotoxicity and significant *in vivo* anticancer activity. As drug carriers, the Curc-OEG nanoparticles could carry other anticancer drugs, such as doxorubicin (DOX) and camptothecin (CPT), to synergize their anticancer efficacies.

Materials & methods

Cell lines

The human ovarian carcinoma SKOV-3 cell line and OVCAR cell line, MCF-7 breast cancer cell lines, were purchased from American Type Culture Collection (ATCC). The drug resistance MCF-7/ADR breast cancer cell line was kindly supplied by Meihua Sui at the Medical University of South Carolina (SC, USA). Cells were propagated in T-75 flasks under an atmosphere of 5% CO_2 at 37°C and grown in Roswell Park Memorial Institute (RPMI) 1640 medium supplemented with 10% fetal bovine serum (HyClone, Logan, UT, USA)

Cytotoxicity assay

The cytotoxicity of Curc-OEG was determined by standard 3-(4,5-dimethylthiazol-2-yl)-2,5-diphenyltetrazolium bromide (MTT) assay using MTT cell proliferation kit (ATCC, Manassas, VA, USA). In brief, cells were seeded onto 96-well plates (4000 cells/well) and incubated at 37°C for 24 h. The medium in each well was replaced with 200 µl of culture medium containing the treatments and the cells were cultured for 72 h. The treatment in each well was then replaced with 200 µl fresh medium and the cells were incubated for another 24 h. A total of 10 µl of MTT reagent was added to each well, followed by addition of 100 µl of detergent reagent 6 h later. The plate was incubated for another 18 h in dark and then read at 570 nm on a Bio-Rad (model 550) microplate reader. Parent curcumin was dissolved in dimethyl sulfoxide and then diluted in medium for MTT assay. The cytotoxicity of PEG454 methyl ether acrylate and mercaptopropionic acid were also measured. The cytotoxicity of DOX and the Curc-OEG nanoparticles loaded with DOX against MCF-7/ADR cells were determined based on 24 h treatment and 24 h postreatment time.

Cellular uptake of the Curc-OEG nanoparticles loaded with DOX

MCF-7/ADR cells were seeded into glass bottom Petri dishes (MatTek, Ashland, MA, USA) at 75,000 cells per plate in 2 ml of RPMI-1640

medium containing 10% FBS. The cells were incubated for 24 h and then the medium was replaced with 2 ml of fresh medium containing either 2 µg/ml free DOX (based on DOX base) or Curc-OEG (50 µg/ml) nanoparticles loaded with 2 µg/ml DOX base. After the cells were cultured for 4 h, the medium was then removed and the cells were washed with PBS. The cellular uptake was observed using a Leica TCS SP2 microscope. DOX was excited with 488 nm Ar/Arkr laser and the emitting wavelength was set from 560 to 600 nm.

Animals

Athymic nude mice (BALB/c nu/nu, Charles River Laboratories, Wilmington, MA, USA) were maintained in compliance with the policy on animal care expressed in the National Research Council guidelines and all experiments were approved and supervised by the Institutional Animal Care and Use Committee (IACUC) at the University of Wyoming (WY, USA). Mice were maintained in a pathogen-free environment under controlled temperature (24°C) and lighting (12L:12D) conditions. Autoclaved rodent chow and sterilized water were supplied *ad libitum*.

Antitumor activity against SKOV-3 ovarian carcinoma intraperitoneal xenografts

Briefly, SKOV-3 cells (5×10^6 suspended in 0.2 ml PBS) were injected into the abdominal cavity of mature nude mice. After 5 weeks, the mice were randomly divided into a treatment group and a control group (n = 9). Curc-OEG in 0.1 ml PBS at a 25 mg/kg dose was injected via the tail vein to the treatment group mice and 0.1 ml PBS was injected to each of the control group mice. The parent curcumin group was not included as a control because it is water insoluble and cannot be dispersed in PBS for intravenous injection. All visible tumors were dissected at necropsy 48 h following the treatments. Cumulative wet tumor weights and tumor numbers per mouse were determined. Samples of tumors, liver, spleen, kidney, heart, intestine and brain were prepared for light microscopic examination.

Antitumor activity against MDA-MB-468 breast cancer subcutaneous xenografts

A 100-µl cell suspension in PBS containing 5×10^6 MDA-MB-468 cells was injected into the mammary fat pads of BALB/c female nude mice. A total of 2 weeks later, when the tumor reached approximately 5 mm in size, the mice were randomly divided into two groups (n =11). The treatment group was injected intravenously with Curc-OEG in 0.1 ml PBS at a 25 mg/kg dose and the control group was injected with 0.1 ml of PBS. The tumors were dissected 48 h after the treatments and weighed. The difference in tumor weight between the control and treatment groups was used as an overall mark of antitumor activity of Curc-OEG against the MDA-MB-468 xenografts.

Statistics analysis

Assignments to treatments and selections of microscopic fields were made at random. Treatment comparisons were made by analysis of variance and protected least significant difference or Student's t-test. Contrasts were considered different at p-values of less than 0.05. Data are presented as means ± standard errors.

Results & discussion

Design & synthesis of Curc-OEG

Curcumin's low bioavailability is primarily due to its extremely low water solubility and instability at the physiological pH. Curcumin conjugates can be made water soluble by introducing water-soluble dendrimers [37] or long PEG chains [38], but the high molecular weights of these macromolecular carriers caused low drug-loading contents. We proposed that curcumin conjugated with small water-soluble moieties would not be molecularly water soluble, but would be similar to an amphiphilic surfactant that dissolves in water as micelles (core-shell nanoparticles). Their core would be solely made of the hydrophobic curcumin moieties, leading to high and fixed curcumin-loading content. The hydrophobic environment of the core in turn stabilizes the curcumin. Furthermore, the nanosized micelles could target tumor tissues by passive accumulation via the enhanced permeability and retention of tumors [39]. Since curcumin can quickly decompose at the neutral or basic conditions, it is preferable for the curcumin-conjugate to be stable in blood compartments to form the micelles, but hydrolyzable to release curcumin in cancer tissues or cytosol for therapeutic effects. We found that the β-thioesters of some phenols were stable in the neutral conditions, but labile in the presence of thiols or esterase. The concentration of reduced glutathione (GSH) was found in a range of 0.5 to 10 mM in cancer cells, but generally just few micromoles per liter in blood plasma [40]. The

esterase is primarily localized in various organ tissues (from tens of units to thousands of units) but very low in serum (several units) [41].

Accordingly, we designed a curcumin-based surfactant (Curc-OEG) by conjugating two very short OEG chains via β-thioester bonds (Figure 1A). Its synthesis is shown in Figure 1B (see Supplementary Figures 1–4 for the procedure and characterizations; available online at www.futuremedicine.com/toc/nnm/5/6). Curc-OEG contained 25.3 wt% curcumin.

Formation of micelles (nanoparticles)

Curc-OEG had very good solubility in water (>50 mg/ml). Its critical micelle concentration, determined by a fluorescence method, was 50 μg/ml (Supplementary Figure 5). The micelles had an average diameter of 37±3.4 nm and a zeta potential of approximately -20 mV (Supplementary Figure 6).

Release of curcumin

As illustrated in Figure 1C, Curc-OEG was considerably stable in PBS at pH 7.4 or 5.0. Less than 12% of Curc-OEG hydrolyzed in 24 h. The presence of GSH significantly promoted the hydrolysis. In the presence of 2 mM GSH, more than 25% at pH 7.4 and 35% at pH 5.0 of Curc-OEG hydrolyzed within 10 h. Esterase greatly accelerated its hydrolysis. At an esterase concentration of 30 U at pH 7.4, more than 80% of Curc-OEG hydrolyzed within 2 h. The released curcumin was found to be the same as the parent curcumin, as detected by high-performance liquid chromatography.

Curc-OEG was found to quickly enter SKOV-3 cells, as observed by confocal microscopy (Supplementary Figure 7). Curc-PEG selectively localized in the lysosomes of SKOV-3 cells after 0.5 h incubation at a dose of 5 μg/ml. At a high dose of 50 μg/ml, Curc-PEG appeared to be localized in the cytoplasm and various compartments in cytoplasm but not in the nucleus, even after 2-h incubation. The localization of Curc-PEG in lysosomes implied Curc-PEG might be taken up by endocytosis of its nanoparticles, which is a general pathway for nanoparticles.

These results imply that the designed Curc-OEG is stable in blood circulation but quickly hydrolysable to release curcumin in the cytosol by the intracellular GSH and/or esterase.

Curc-OEG as an anticancer prodrug

In Curc-OEG, the releasable curcumin is the active component. Since curcumin interacts with a wide variety of cell signaling proteins, we only selected the several most relevant to cell inhibition to analyze its biological activities and compared it with parent curcumin.

Cell-cycle arrest caused by Curc-OEG

Oncogene-induced overexpression of cyclin D1 is associated with tumorigenesis. Cyclin D1 partners with cyclin-dependent kinases CDK4 and CDK6 and functions as a regulatory factor that modulates the progression of cell cycles from G1 phase to S phase [42,43]. The effects of Curc-OEG on the Cyclin D1, CDK4 and CDK6 expressions were examined by western blotting analysis (Figure 2A). Obviously, the three essential proteins were significantly down-regulated in a dose-dependent fashion after treatment with Curc-OEG, and the 20 μg/ml dose completely inhibited the cyclin D1 and CDK4 expression, which clearly indicated that Curc-OEG could arrest SKOV-3 cell cycles at G0/G1 phase.

Apoptosis induced by Curc-OEG

The induction of cell apoptosis by Curc-OEG and curcumin was further detected by Hoechst staining (Figure 2B). Obviously, progressive increases in relative percentages of apoptotic SKOV-3 cells occurred at 12, 24 and 36 h after treatment with Curc-OEG or curcumin. The Curc-OEG evoked apoptosis at a slower rate than native curcumin at an equivalent dose, which could be attributed to the hydrolysis process of Curc-OEG. Significant apoptosis elevations above control were not observed until 24 h post-treatment. Almost complete cell death was detected by 48 h for both curcumin and Curc-OEG. The induction of cell apoptosis indicated Curc-OEG could be a potential cytotoxin against SKOV-3 and other cancer cells.

In vitro cytotoxicity of Curc-OEG by MTT assay

The cytotoxicities of Curc-OEG against cancer cell lines, including SKOV-3 and OVCAR ovarian cancer cells, MCF-7 and MDA-MB-468 beast cancer cells and K12 colon cancer cells, were subsequently assessed using standard MTT assay (Figure 2C). Obviously, Curc-OEG showed significant cytotoxicities to all the investigated cell lines. The OEG used for synthesizing Curc-OEG was found to have no distinct cytotoxicity (data not shown). The half maximal inhibitory concentration (IC_{50}) ranged from 1.4 μg/ml (for MDA-MB-468) to 7.8 μg/ml (for MCF-7) curcumin-equivalent doses (Table 1), indicating that Curc-OEG has a

broad-spectrum of anticancer activities against tumor cells of human origin. In addition, Curc-OEG clearly demonstrated enhanced cytotoxicity compared with free curcumin. For example, the IC_{50} against SKOV-3 cells was 4.4 µg/ml for Curc-OEG but was 7.6 µg/ml for parent curcumin.

Blood clearance & tissue distribution

Administration of parent curcumin can only produce very low curcumin levels in serum and tissues. For example, no curcumin was found in heart blood of rats orally administrated 400 mg of curcumin [44]. Mice intraperitoneally injected with 100 mg/kg curcumin had a peak plasma level of 2.25 µg/ml[45]. Intravenous administration of curcumin is difficult except when using organic solvents [17]. Intravenously injected curcumin was quickly cleaned from the blood circulation within 1 h after injection [46]. Rats intravenously injected with 10 mg/kg curcumin had a maximum serum level of 0.36 µg/ml [47]. By contrast, as shown in Figure 3A, the intravenously injected Curc-OEG at a low dose of 25 mg/kg (6.25 mg/kg curcumin-equivalent dose) gave a 6.8 µg/ml level of curcumin in the plasma. Even though the curcumin concentration quickly decreased in 1 h, the plasma still maintained 0.1–0.2 µg/ml of curcumin level 2 h after the injection. Thus, the intravenously injected Curc-OEG could produce approximately 50–500-times higher plasma curcumin level than orally, intravenously or intraperitoneally administrated curcumin.

The curcumin tissue distribution of the mice intravenously administrated with 25 mg/kg of Curc-OEG is shown in Figure 3B. Unlike intraperitoneal or orally administrated curcumin, most of which was located in the gastrointestinal area or was expelled from the mouse body [29], the intravenously injected Curc-OEG gave a high concentration of curcumin in liver, spleen and tumor tissues. Only small amounts of curcumin was distributed in intestine, kidney and brain. Most importantly, the intravenously injected Curc-OEG at 6.25 mg/kg curcumin-equivalent dose led to several micrograms of curcumin per gram of tissue in tumor tissues. The curcumin concentration in spleen decreased while that in the tumor tissue further increased to above 8 µg/g after 1 h. This is a significant improvement compared with the reported results that the curcumin concentrations in tumor tissues were usually very low when curcumin was administrated. The improved curcumin bioavailability in tumor may be because the Curc-OEG-formed micelles stabilized curcumin, prolonged the blood circulation time, and targeted to the tumors by passive accumulation via the enhanced permeability and retention effect.

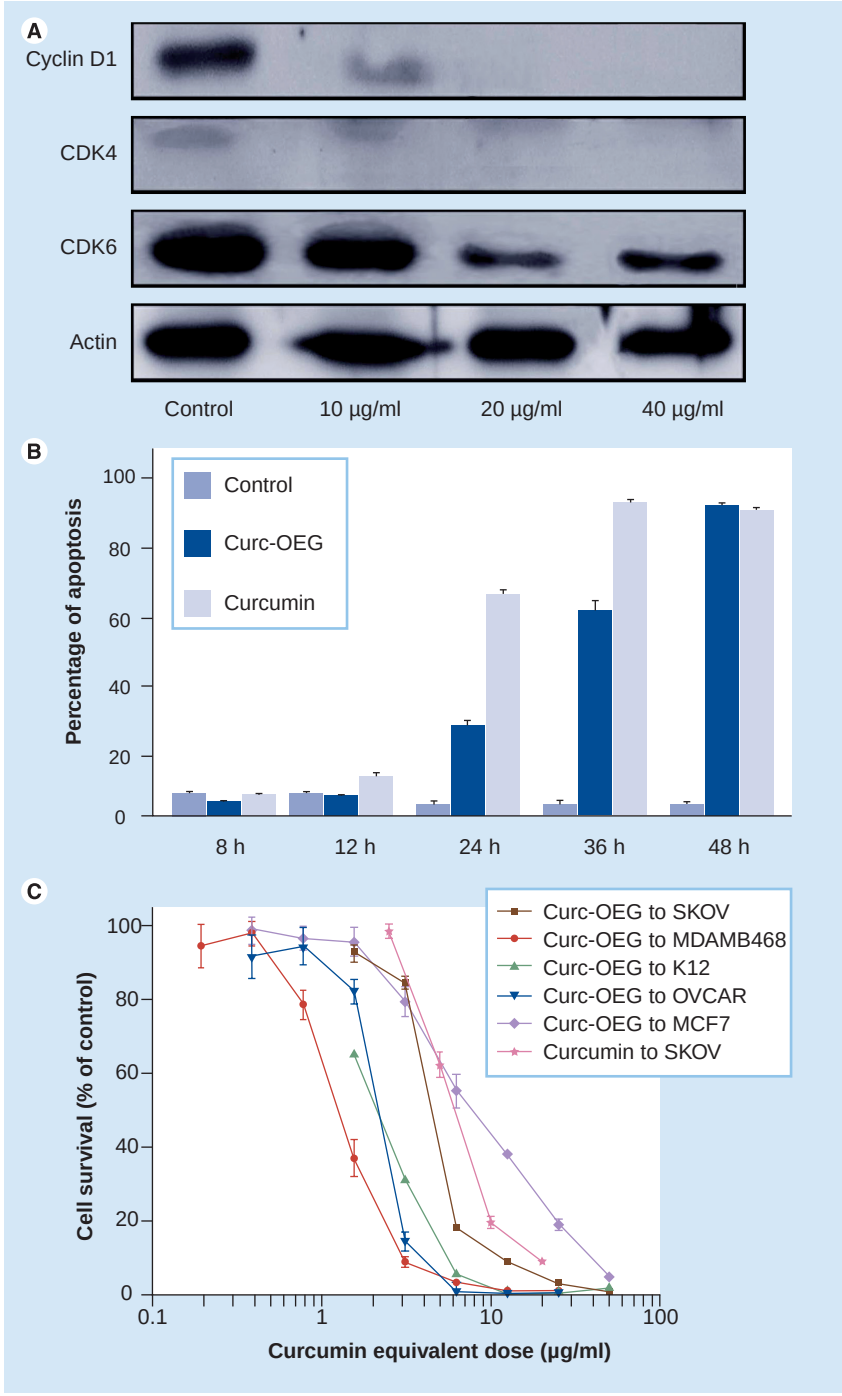

Figure 2. Curc-OEG-induced cell apoptosis and cytotoxicity.
(A) Western blotting analysis of cyclin D1, CDK4 and CDK6 expression of SKOV-3 cells treated with 10, 20 and 40 µg/ml of Curc-OEG for 24 h. **(B)** *In vitro* effects of free curcumin and Curc-OEG on apoptosis of SKOV-3 cells treated with 25 µg/ml curcumin or 100 µg/ml Curc-OEG (25.3 µg/ml curcumin equivalent). **(C)** Dose–response curves of Curc-OEG against cancer cell lines after 72 h treatment and 24 h postreatment.
Curc-OEG: Curcumin conjugated with two oligo(ethylene glycol) chains.

Table 1. IC_{50} of curcumin conjugated with two oligo(ethylene glycol) chains against SKOV-3, OVCAR, MCF-7, MDA-MB-468 and K12 cancer cell lines.

Cell line	SKOV	MCF-7	K12	MDA-MB-468	OVCAR
IC_{50} (μg/ml)†	4.4	7.8	2.0	1.4	1.8

†*Based on curcumin equivalent dose; curcumin equivalent dose = dose of curcumin conjugated with two oligo(ethylene glycol) chains × 25.3%.*

Acute & subchronic toxicity of Curc-OEG

Even though there were high concentrations of curcumin in liver and spleen, the subsequent systemic toxicity investigations indicated that Curc-OEG inherited the merit from parent curcumin. In the acute toxicity study, all mice that received a single dose of 100 or 250 mg/kg showed no sign of acute toxicity as evidenced by the mice normal body appearance, respiratory pattern and frequency of movement. In subchronic toxicity study, repeated doses of 100 or 250 mg/kg did not change the animal's general behavior and autonomic signs and caused no morbidity or mortality in the mice. There were no significant differences in the weekly mean bodyweight and no significant differences in the histology of vital organ tissues, such as the liver, between the control group and the treatment group (Supplementary Figure 8).

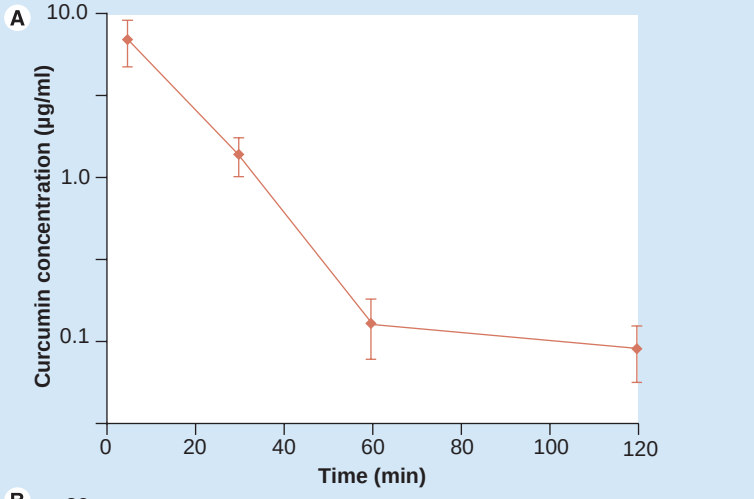

Figure 3. Curc-OEG's blood clearance and biodistribution. (A) The time course of the curcumin plasma clearance of the mice intravenously injected with 25 mg/kg curcumin conjugated with two oligo(ethylene glycol) chains and **(B)** their curcumin tissue distributions. Mice were sacrificed and tissues were collected 0.5 and 1 h, respectively, after the injection.

In vivo antitumor activity against SKOV-3 carcinoma xenografts & MDA-MB-468 xenografts

The *in vivo* antitumor activity of Curc-OEG was afterwards assessed first using the SKOV-3 intraperitoneal xenograft model. Mice were intravenously injected with Curc-OEG at a single dose of 25 mg/kg and the tumors were dissected at necropsy 48 h following the injection since the *in vitro* apoptosis analysis indicated that complete cell apoptosis occurred 48 h after treatment. Figure 4A compares the average tumor weight and tumor number between the treatment and the PBS control groups (the curcumin group was not included because it is water insoluble and cannot be dispersed well in PBS for intravenous injection). Obviously, the Curc-OEG demonstrated strong *in vivo* antitumor activity. The control group had a tumor burden per mouse of 2.68 g, while the Curc-OEG treated group had a tumor burden per mouse of 0.77 g.

Sections of the tumor tissues of the treatment group mice had many cavitated areas (Figure 4B). The appearance of cavitation suggested cell detachments from the extracellular matrix, autophagocytosis and resorption [48]. Indeed, there was evidence that curcumin could activate autophagy and that there was interplay between mechanisms of apoptosis and autophagy [49].

The *in vivo* antitumor activity of Curc-OEG was further corroborated by subcutaneous (mammary fat pad) xenograft studies using MDA-MB-468 breast cancer cells (Figure 4C). A single dose of Curc-OEG (25 mg/kg) also surprisingly reduced approximately 50% of tumor growth, strongly demonstrating that the Curc-OEG indeed had remarkable *in vivo* tumor suppression and inhibitory effects.

Thus, Curc-OEG is an intravenous-injectable, water-soluble curcumin derivative with strong *in vivo* antitumor effects. The strong tumor suppression and inhibitory effects are agreeable with the high curcumin concentration in tumors after Curc-OEG was administrated. The remarkably high bioavailability of curcumin may account for the tumor suppression by Curc-OEG.

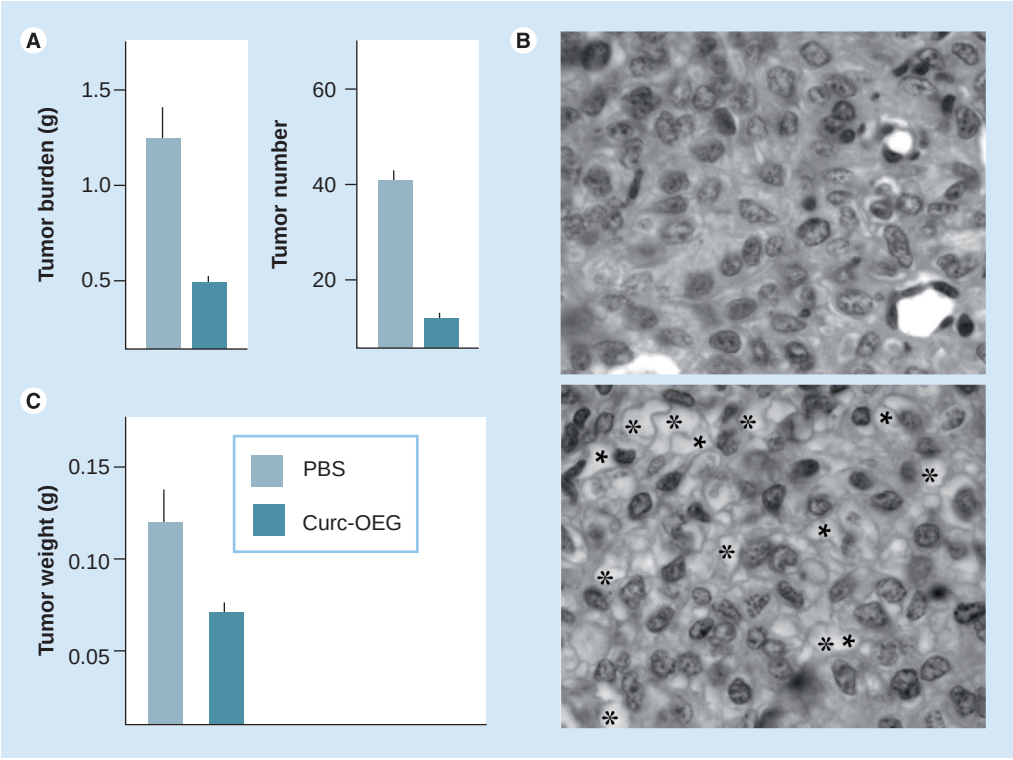

Figure 4. *In vivo* antitumor activity. (A) *In vivo* antitumor activity of Curc-OEG against SKOV-3 carcinoma xenografts to mice, the tumor tissue sections from the mice treated with (**B**: lower panel) Curc-OEG or (**B**: upper panel) PBS control, and **(C)** *in vivo* antitumor activity of Curc-OEG against MDA-MB-468 carcinoma xenografts model. Mice were intravenously injected with 25 mg/kg Curc-OEG or 0.1 ml PBS control and the tumors were dissected at necropsy 48 h following the injection.
Curc-OEG: Curcumin conjugated with two oligo(ethylene glycol) chains; PBS: Phosphate buffered saline.

Curc-OEG nanoparticles as drug carriers

Nanoparticles loaded with other drugs

Curc-OEG formed micelles of approximately 37 nm in diameter. The formed micelles/nanoparticles could be used as carriers for anticancer drugs, such as DOX and CPT. The loading contents determined by HPLC were 57 μg/ml for DOX and 36 μg/ml for CPT, with corresponding loading efficiencies of 57 and 36%, respectively. Figure 5A shows the size distributions of nanoparticles before and after drug loading measured by dynamic light scattering. Obviously, the size increased from 37 to 157 or 99 nm after loading with DOX or CPT. The transmission electron microscopy results confirmed the nanoparticle structures (Supplementary Figure 9).

Synergic effects between Curc-OEG & loaded DOX

The *in vitro* cytotoxicities of the DOX-loaded Curc-OEG nanoparticles against DOX-resistant MCF-7/ADR cells were estimated by MTT assay. As shown in Figure 5B, the MCF-7 ADR cells treated with Curc-OEG (100 μg/ml) had approximately 45% viability compared with control. The DOX (5.0 μg/ml) alone killed approximately 56% of the cells. However, the Curc-OEG nanoparticles (100 μg/ml) loaded with 5.0 μg/ml DOX almost completely eliminated MCF-7 ADR cells (~2% viability), which suggested the Curc-OEG carrier enhanced the cytotoxicity of loaded DOX. Therefore, DOX and Curc-OEG had a strong synergetic cytotoxicity to MCF-7 ADR cells. This result is agreeable with the reports that curcumin could potentiate chemotherapy [24,25].

The cellular uptake of free and encapsulated DOX was observed by confocal fluorescence microscopy. Curc-OEG micelles significantly enhanced the cellular internalization of DOX into MCF-7/ADR cells (Figure 5C). No free DOX (pseudo-colored blue) appeared in the MCF-7/ADR cells after the cells were incubated with 2 μg/ml of DOX for 4 h, while DOX loaded in Curc-OEG micelles at the same DOX dose

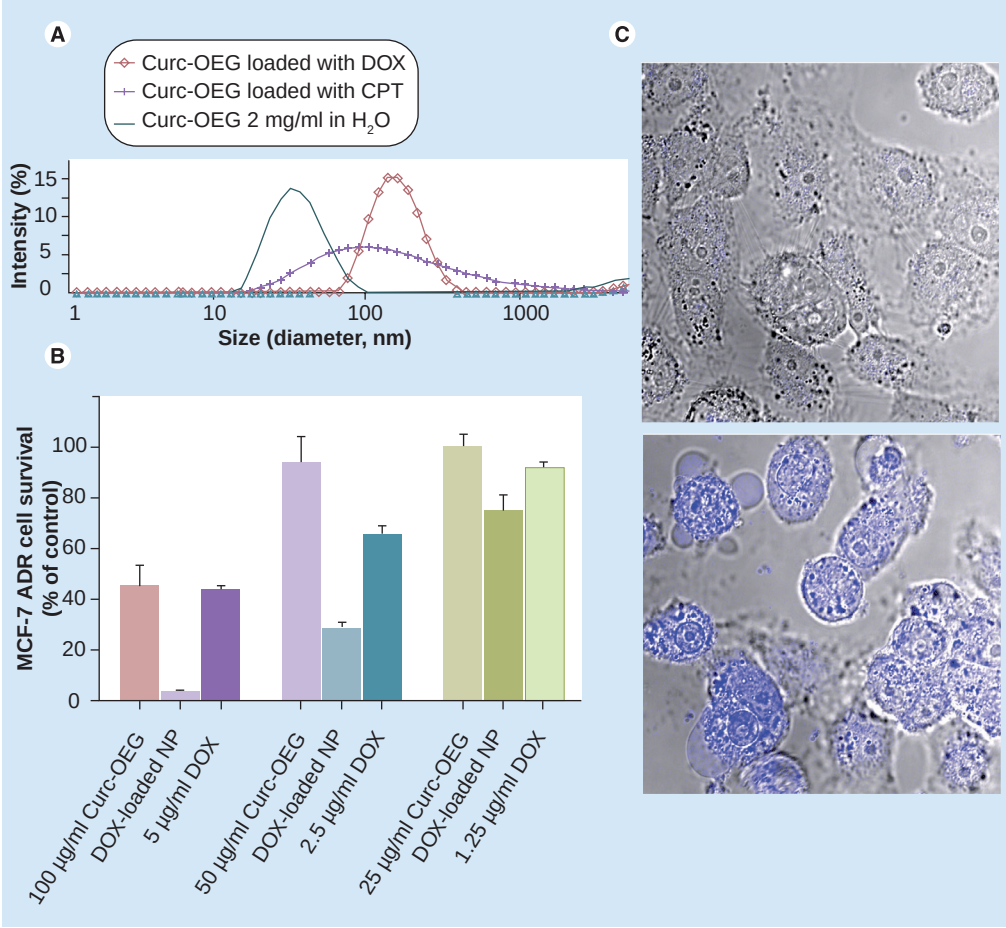

Figure 5. Curc-OEG as drug carriers. (A) Size distributions of Curc-OEG NPs before and after loaded with DOX or CPT, **(B)** *in vitro* synergetic effect between the Curc-OEG and the loaded DOX, and **(C)** cellular uptake of free DOX (upper panel) and the Curc-OEG NPs loaded with DOX (lower panel, 50 mg/ml Curc-OEG with 2mg/ml of DOX).
CPT: Camptothecin; Curc-OEG: Curcumin-oligo(ethylene glycol) conjugate; DOX: Doxorubicin; NP: Nanoparticle.

could efficiently enter the cells in 4 h. This may be because these large nanoparticles enter cells via endocytosis, bypassing the membrane-associated drug resistance [50], and the release curcumin downregulated MDR proteins [8]. Thus, the improved cellular uptake of the DOX loaded in Curc-OEG micelles partially accounted for its enhanced cytotoxicity compared with free DOX.

Conclusion

The surfactant-like amphiphilic Curc-OEG formed micelles with two roles – as an anticancer prodrug and as a drug carrier. This curcumin prodrug has a fixed composition with a curcumin-loading content of 25.3 wt% and can release curcumin once in the cytosol. It alone showed broad *in vitro* antitumor activities against several cancer cell lines of human origin. *In vivo*, it had no acute and subchronic systemic toxicity, but remarkably improved bioavailability, and significant tumor inhibition and suppression activities in both the SKOV-3 intraperitoneal and MDA-MB-468 subcutaneous xenograft models. As drug carriers, Curc-OEG micelles can carry other drugs, such as DOX and CPT, and ship them into drug-resistant cells. Strong synergic effects were found between Curc-OEG and the loaded DOX. Thus, Curc-OEG is an intravenous-injectable, water-soluble curcumin prodrug that merits further study in cancer therapy. The *in vivo* anticancer activity of multiple treatments and cancer prevention of Curc-OEG, and its synergic effect with DOX are currently under investigation and will be reported elsewhere.

Future perspective

Curcumin is referred to as a 'magic' medicine in terms of its nontoxicity to healthy tissues and also a wide range of biological activities. However, it is still useless in clinic due

to its extremely low bioavailability caused by its low water solubility and instability. This amphiphilic curcumin prodrug, Curc-OEG, may provide a viable approach to solve this problem. Compared with other curcumin delivery systems, whose compositions vary from batch to batch, making them difficult to be formulated as medicines, the prodrug can be easily formulated as nanoparticles with a fixed composition. This study demonstrates that the prodrug produces a high curcumin bioavailability and thus, a high anticancer activity. Future research will be needed to study *in vivo* anticancer activity of multiple treatments and cancer prevention of Curc-OEG, and its synergic effect with DOX.

Acknowledgements

Technical assistance provided by Kellee Sundstrom, Dale Isaak, Kathleen Austin, Robbie Schamber and Jessica Coonts at the University of Wyoming (WY, USA) is appreciated.

Financial & competing interests disclosure

The authors thank the National Science Foundation (NSF-CBET 0753109), NIH (RR-016474) and Department of Defense (BC0083821) of USA, and the National Basic Research Program (973 Program, 2009CB526403), National Natural Science Foundation (20974096) and National Fund for Distinguished Young Scholars (50888001) of China for financial supports. ***The authors have no other relevant affiliations or financial involvement with any organization or entity with a financial interest in or financial conflict with the subject matter or materials discussed in the manuscript apart from those disclosed.***

No writing assistance was utilized in the production of this manuscript.

Ethical conduct of research

The authors state that they have obtained appropriate institutional review board approval or have followed the principles outlined in the Declaration of Helsinki for all human or animal experimental investigations. In addition, for investigations involving human subjects, informed consent has been obtained from the participants involved.

Executive summary

Curcumin-oligo(ethylene glycol) conjugate was explored to improve curcumin's bioavailability

- Curcumin-oligo(ethylene glycol) conjugate (Curc-OEG) was synthesized by dicyclohexylcarbodiimide-catalyzed esterification.
- Curc-OEG formed micelles (nanoparticles) with a diameter of 37 nm, a CMC of 50 μg/ml, and a high and fixed curcumin loading (25.3 wt%).
- Curc-OEG and was stable in the blood but hydrolyzed to release active curcumin once in cytosol due to the presence of glutathione or esterase.

Curc-OEG showed broad* in vitro *antitumor activities against a series of cancer cell lines of human origin

- Curc-OEG inhibited the cyclin D1 and CDK4 expression and arrested SKOV-3 cell cycle at G0/G1 phase.
- Curc-OEG induced cell apoptosis and reached the same activity as curcumin at 48 h culture.
- Curc-OEG had enhanced cytotoxicity compared with free curcumin to SKOV-3, MDA-MB-468, MCF-7 and K12 cancer cell lines.

In vivo*, Curc-OEG demonstrated significant tumor inhibition & suppression activities in both the SKOV-3 intraperitoneal & MDA-MB-468 suncutaneous xenograft models*

- Curc-OEG intravenously injected to mice had a long blood circulation time and produced approximately 50–500-times higher plasma curcumin level than orally, intervenously or intraperitonealy administrated curcumin.
- Curcu-OEG improved curcumin bioavailability, leading to several micrograms of curcumin per gram of tumor tissue.
- Intravenously injected Curc-OEG quickly reduced intraperitoneal SKOV-3 ovarian tumors and subcutaneous MDA-MB-468 breast tumors.
- Curc-OEG demonstrated no acute toxicity and no apparent subchronic toxicity.

As a drug carrier, Curc-OEG nanoparticles could carry other drugs & had strong synergic cytotoxicity with the loaded DOX

- The Curc-OEG nanoparticles could be loaded with other hydrophobic drugs, such as doxorubicin or camptothecin.
- The Curc-OEG nanoparticles carried doxorubicin into MCF-7 ADR cells.
- The loaded DOX and Curc-OEG had a strong synergetic cytotoxicity to MCF-7 ADR cells.

Conclusion

- Amphiphilic Curc-OEG served two roles: an anticancer prodrug and a drug carrier.
- As an anticancer prodrug, Curc-OEG had significantly improved stability, water solubility and bioavailability.
- Curc-OEG showed significant *in vitro* and *in vivo* anticancer activities, and had no acute and subchronic systemic toxicity.
- As a drug carrier, Curc-OEG nanoparticles could carry other drugs and might have synergic effects.

Bibliography

1 Jagtap S, Meganathan K, Wagh V, Winkler J, Hescheler J, Sachinidis A: Chemoprotective mechanism of the natural compounds, epigallocatechin-3-*O*-gallate, quercetin and curcumin against cancer and cardiovascular diseases. *Curr. Med. Chem.* 16, 1451–1462 (2009).

2 Aggarwal BB, Surh YH, Shishodia S: *The Molecular Targets and Therapeutic Uses of Curcumin in Health and Disease*. Springer, NY, USA (2007).

3 Strimpakos AS, Sharma RA: Curcumin: preventive and therapeutic properties in laboratory studies and clinical trials. *Antioxid. Redox Signaling* 10, 511–546 (2008).

4 Lin YG, Kunnumakkara AB, Nair A *et al.*: Curcumin inhibits tumor growth and angiogenesis in ovarian carcinoma by targeting the nuclear factor-kB pathway. *Clin. Cancer Res.* 13, 3423–3430 (2007).

5 Kunnumakkara AB, Anand P, Aggarwal BB: Curcumin inhibits proliferation, invasion, angiogenesis and metastasis of different cancers through interaction with multiple cell signaling proteins. *Cancer Lett.* 269 199–225 (2008).

6 Karunagaran D, Rashmi R, Kumar TR: Induction of apoptosis by curcumin and its implications for cancer therapy. *Curr. Cancer Drug Target* 5, 117–129 (2005).

7 Rajesh LT, Anuj S, Radha KM: Multiple molecular targets in cancer chemoprevention by curcumin. *AAPS J.* 8, E443–E449 (2006).

8 Shukla S, Zaher H, Hartz A, Bauer B, Ware JA, Ambudkar SV: Curcumin inhibits the activity of ABCG2/BCRP1, a multidrug resistance-linked ABC drug transporter in mice. *Pharm. Res.* 26, 480–487 (2009).

9 Zhang W, Tan TMC, Lim L-Y: Impact of curcumin-induced changes in P-glycoprotein and CYP3A expression on the pharmacokinetics of peroral celiprolol and midazolam in rats. *Drug Metab. Dispos.* 35, 110–115 (2006).

10 Li L, Ahmed B, Mehta K, Kurzrock R: Liposomal curcumin with and without oxaliplat, effects on cell growth, apoptosis, and angiogenesis in colorectal cancer. *Mol. Cancer Ther.* 6, 1276–1282 (2007).

11 Dorai T, Cao YC, Dorai B, Buttyan R, Katz AE: Therapeutic potential of curcumin in human prostate cancer. III. Curcumin inhibits proliferation, induces apoptosis, and inhibits angiogenesis of LNCaP prostate cancer cells *in vivo*. *Prostate* 47 293–303 (2001).

12 Somers-Edgar TJ, Scandlyn MJ, Stuart EC, Le Nedelec MJ, Valentine SP, Rosengren RJ: The combination of epigallocatechin gallate and curcumin suppresses ERα -breast cancer cell growth *in vitro* and *in vivo*. *Int. J. Cancer* 122, 1966–1971 (2008).

13 Narayanan Narayanan K, Nargi D, Randolph C, Narayanan Bhagavathi A: Liposome encapsulation of curcumin and resveratrol in combination reduces prostate cancer incidence in PTEN knockout mice. *Int. J. Cancer* 125, 1–8 (2009).

14 Milacic V, Banerjee S, Landis-Piwowar KR, Sarkar FH, Majumdar APN, Dou QP: Curcumin Inhibits the proteasome activity in human colon cancer cells *in vitro* and *in vivo*. *Cancer Res.* 68, 7283–7292 (2008).

15 Dujic J, Kippenberger S, Ramirez-Bosca A *et al.*: Curcumin in combination with visible light inhibits tumor growth in a xenograft tumor model. *Int. J. Cancer* 124, 1422–1428 (2009).

16 William BM, Goodrich A, Peng C, Li S: Curcumin inhibits proliferation and induces apoptosis of leukemic cells expressing wild-type or T315I-BCR-ABL and prolongs survival of mice with acute lymphoblastic leukemia. *Hematology* 13, 333–343 (2008).

17 Purkayastha S, Berlinerb A, Fernandoa SS *et al.*: Curcumin blocks brain tumor formation. *Brain Res.* 1266, 130–138 (2009).

18 Shankar S, Ganapathy S, Chen Q, Srivastava RK: Curcumin sensitizes TRAIL-resistant xenografts: molecular mechanisms of apoptosis, metastasis and angiogenesis. *Mol. Cancer* 7, 16 (2008).

19 Ajaikumar BK, Preetha A, Bharat BA: Curcumin inhibits proliferation, invasion, angiogenesis and metastasis of different cancers through interaction with multiple cell signaling proteins. *Cancer Lett.* 269 199–225 (2008).

20 Chen H-W, Lee J-Y, Huang J-Y *et al.*: Curcumin inhibits lung cancer cell invasion and metastasis through the tumor suppressor HLJ1. *Cancer Res.* 68, 7428–7438 (2008).

21 Narasimhan M, Ammanamanchi S: Curcumin blocks RON tyrosine kinase-mediated invasion of breast carcinoma cells. *Cancer Res.* 68, 5185–5192 (2008).

22 Kunnumakkara AB, Diagaradjane P, Guha S *et al.*: Curcumin sensitizes human colorectal cancer xenografts in nude mice to γ-radiation by targeting nuclear factor-kB-regulated gene products. *Clin. Cancer Res.* 14, 2128–2136 (2008).

23 Javvadi P, Segan a T, Tuttle SW, Koumenis C: The chemopreventive agent curcumin is a potent radiosensitizer of human cervical tumor cells via increased reactive oxygen species production and overactivation of the mitogen-activated protein kinase pathway. *Mol. Pharmacol.* 73, 1491–1501 (2008).

24 Kunnumakkara a B, Guha S, Krishnan S, Diagaradjane P, Gelovani J, Aggarwal BB: Curcumin potentiates antitumor activity of gemcitabine in an orthotopic model of pancreatic cancer through suppression of proliferation, angiogenesis, and inhibition of nuclear factor-κB-regulated gene products. *Cancer Res.* 67, 3853–3861 (2007).

25 Kamat AM, Sethi G, Aggarwal BB: Curcumin potentiates the apoptotic effects of chemotherapeutic agents and cytokines through downregulation of nuclear factor-κB and nuclear factor-κB-regulated gene products in IFN-α -sensitive and IFN-α -resistant human bladder cancer cells. *Mol. Cancer Ther.* 6, 1022–1030 (2007).

26 Cheng AL, Hsu CH, Lin JK *et al.*: Phase I clinical trial of curcumin, a chemopreventive agent, in patients with high-risk or pre-malignant lesions. *AntiCancer Res.* 21, 2895–2900 (2001).

27 Sharma R A, Euden SA, Platton S L *et al.*: Phase I clinical trial of oral curcumin: biomarkers of systemic activity and compliance. *Clin. Cancer Res.* 10, 6847–6854 (2004).

28 Dhillon N, Aggarwal BB, Newman RA *et al.*: Phase II trial of curcumin in patients with advanced pancreatic cancer. *Clin. Cancer Res.* 14, 4491–4499 (2008).

29 Anand P, Kunnumakkara AB, Newman RA, Aggarwal BB: Bioavailability of curcumin: problems and promises. *Mol. Pharm.* 4, 807–818 (2007).

30 Wang Y-J, Pan M-H, Cheng A-L *et al.*: Stability of curcumin in buffer solutions and characterization of its degradation products. *J. Pharm. Biomed. Anal.* 15, 1867–1876 (1997).

31 Liang G, Shao L, Wang Y *et al.*: Exploration and synthesis of curcumin analogues with improved structural stability both *in vitro* and *in vivo* as cytotoxic agents. *Bioorg. Med. Chem.* 17, 2623–2631 (2009).

32 Youssef D, Nichols CE, Cameron TS, Balzarini J, De Clercq E, Jha A: Design, synthesis, and cytostatic activity of novel cyclic curcumin analogues. *Bioorg. Med. Chem. Lett.* 17, 5624–5629 (2007).

33 Chen C, Johnston TD, Jeon H *et al.*: An *in vitro* study of liposomal curcumin: stability, toxicity and biological activity in human lymphocytes and Epstein–Barr virus-transformed human B-cells. *Int. J. Pharm.* 366, 133–139 (2009).

34 Shankeshi J, Aukunuru J: Preparation, characterization and evaluation of antidiabetic activity of a liposomal formulation encapsulating curcumin, an ayurvedic natural product. *Pharmacist (Bhopal, India)* 3, 1–5 (2008).

35 Marczylo TH, Verschoyle RD, Cooke DN, Morazzoni P, Steward W P, Gescher a J: Comparison of systemic availability of curcumin with that of curcumin formulated with phosphatidylcholine. *Cancer Chemother. Pharmacol.* 60, 171–177 (2007).

36 Bisht S, Feldmann G, Soni S *et al.*: Polymeric nanoparticle-encapsulated curcumin ("nanocurcumin"): a novel strategy for human cancer therapy. *J. Nanobiotechnol.* 5, 1–18 (2007).

37 Shi W, Dolai S, Rizk S *et al.*: Synthesis of monofunctional curcumin derivatives, clicked curcumin dimer, and a PAMAM dendrimer curcumin conjugate for therapeutic applications. *Org Lett.* 9, 5461–5464 (2007).

38 Safavy A, Raisch KP, Mantena S *et al.*: Design and development of water-soluble curcumin conjugates as potential anticancer agents. *J. Med. Chem.* 50, 6284–6288 (2007).

39 Maeda H, Wu J, Sawa T, Matsumura Y, Hori K: Tumor vascular permeability and the EPR effect in macromolecular therapeutics: a review. *J. Control. Release* 65, 271–284 (2000).

40 Meister A, Anderson M: Glutathione. *Ann. Rev. Biochem.* 52, 711–760 (1983).

41 Huggins C, Moulton S: Esterases of testis and other tissues. *J. Exp. Med.* 88, 169–179 (1948).

42 Fu M, Wang C, Li Z, Sakamaki T, Pestell RG: Cyclin D1: normal and abnormal functions. *Endocrinology* 145, 5439–5447 (2004).

43 Hengstschlager M, Braun K, Soucek T, Miloloza A, Hengstschlager-Ottnad E: Cyclin-dependent kinases at the G1-S transition of the mammalian cell cycle. *Mut. Res.* 436, 1–9 (1999).

44 Ravindranath V, Chandrasekhara N: Absorption and tissue distribution of curcumin in rats. *Toxicology* 16, 259–265 (1980).

45 Pan M H, Huang T M, Lin JK: Biotransformation of curcumin through reduction and glucuronidation in mice. *Drug Metab. Dispos.* 27, 486–494 (1999).

46 Ireson C, Orr S, Jones DJL *et al.*: Characterization of metabolites of the chemopreventive agent curcumin in human and rat hepatocytes and in the rat *in vivo*, and evaluation of their ability to inhibit phorbol ester-induced prostaglandin E2 production. *Cancer Res.* 61, 1058–1064 (2001).

47 Yang KY, Lin LC, Tseng TY, Wang SC, Tsai TH: Oral bioavailability of curcumin in rat and the herbal analysis from Curcuma longa by LC-MS/MS. *J. Chromatogr. B Anal. Technol. Biomed. Life Sci.* 853, 183–189 (2007).

48 Lock R, Debnath J: Extracellular matrix regulation of autophagy. *Curr. Opin. Cell Biol.* 20, 583–588 (2008).

49 Aoki H, Takada Y, Kondo S, Sawaya R, Aggarwal BB, Kondo Y: Evidence that curcumin suppresses the growth of malignant gliomas *in vitro* and *in vivo* through induction of autophagy: role of Akt and extracellular signal-regulated kinase signaling pathways. *Mol. Pharmacol.* 72, 29–39 (2007).

50 Wong H, Bendayan R, Rauth A, Xue H, Babakhanian K, Wu X: A mechanistic study of enhanced doxorubicin uptake and retention in multidrug resistant breast cancer cells using a polymer-lipid hybrid nanoparticle system. *J. Pharmacol. Exp. Thera.* 317, 1372–1381 (2006).

Biomaterials 31 (2010) 7139–7149

Contents lists available at ScienceDirect

Biomaterials

journal homepage: www.elsevier.com/locate/biomaterials

Curcumin polymers as anticancer conjugates

Appendix 2

Huadong Tang [b], Caitlin J. Murphy [c], Bo Zhang [b], Youqing Shen [a,b,*], Edward A. Van Kirk [c], William J. Murdoch [c], Maciej Radosz [b]

[a] Center for Bionanoengineering and State Key Lab of Chemical Engineering, Department of Chemical and Biological Engineering, Zhejiang University, Hangzhou 310027, China
[b] Department of Chemical and Petroleum Engineering, University of Wyoming, Laramie, WY 82071, USA
[c] Department of Animal Science, University of Wyoming, Laramie, WY 82071, USA

ARTICLE INFO

Article history:
Received 3 April 2010
Accepted 1 June 2010
Available online 29 June 2010

Keywords:
Drug delivery
Curcumin conjugate
Curcumin polymer
In vivo antitumor activity

ABSTRACT

Curcumin has been shown highly cytotoxic towards various cancer cell lines, but its water-insolubility and instability make its bioavailability exceedingly low and thus it generally demonstrates low anticancer activity in *in vivo* tests. Herein, we report a novel type of polymer-drug conjugates — the high molecular weight curcumin polymers (polycurcumins) made by condensation polymerization of curcumin. The polycurcumins as backbone-type conjugates have advantages of high drug loading efficiency, fixed drug loading contents, stabilized curcumin in their backbones, and tailored water-solubility. The polycurcumins may have many potential applications and their antitumor activities are investigated in this work. The polycurcumins are cytotoxic to cancer cells, but a polyacetal-based polycurcumin (PCurc 8) is highly cytotoxic to SKOV-3, OVCAR-3 ovarian cancers, and MCF-7 breast cancer cell lines. It can be quickly taken up by cancer cells into their lysosomes, where PCurc 8 hydrolyzes and releases active curcumin. It arrests SKOV-3 cell cycle at G_0/G_1 phase *in vitro* and induces cell apoptosis partially through the caspase-3 dependent pathway. *In vivo*, intravenously (i.v.) injected PCurc 8 shows remarkable antitumor activity in SKOV-3 intraperitoneal (i.p.) xenograft tumor model.

1. Introduction

Curcumin, 1,7-bis-(4-hydroxy-3-methoxy-phenyl)-hepta-1,6-diene-3,5-dione, has been shown to have a wide range of biological and pharmacological activities [1–6]. Its strong antiproliferative activity has attracted particular interests as potential cancer chemotherapy and prevention reagents [7,8]. Curcumin was shown to interact with many cellular targets such as nuclear factor-kappa B (NF-κB), transcription factor activator protein-1 (AP-1) and many other proteins [9–11]. Curcumin inhibited various interleukins and multiple protein kinases (e.g., PKC, JNK), and suppressed the expression of human epidermal growth factor receptor (HER-2), epidermal growth factor receptor (EGFR), and estrogen receptor (ER) [1,10,12]. Curcumin was also found to down-regulate multi-drug resistance proteins (MDR) and P-glycoprotein (P-gp), and have the potential to overcome multidrug resistance in cancer cells [13,14]. *In vitro*, curcumin demonstrated cytotoxicity against a wide variety of cancer cell lines including DU145 prostate carcinoma, A549 lung carcinoma, and HT29 colon carcinoma with an IC_{50} (50% inhibitory concentration) of about 10–75 μM [15,16]. Some reports showed that curcumin had *in vivo* preventive and therapeutic effects against human tumors [17–19].

On the other hand, curcumin has been proved pharmacologically safe even at very high doses in many clinical studies and various animal models. For example, curcumin showed no toxicity at a daily oral dose as high as 12 g in a phase I clinical trial and had no dose-limiting toxicity in another phase II trial [20,21].

Unfortunately, curcumin is generally found inactive in clinical trials primarily due to its water-insolubility and instability, and thus exceedingly poor bioavailability [22,23]. Curcumin is hydrophobic and practically insoluble in water at acidic conditions while it quickly degrades in neutral and alkaline conditions with a half life ($t_{1/2}$) less than 10 min in PBS at pH 7.2 [24], resulting in extremely low bioavailability in both vascular and oral administration. For example, in patients orally administrated up to 3.6 g curcumin, only low nanomolar levels of curcumin was detected in their peripheral or portal circulation [21]. This low bioavailability causes curcumin inactive to inhibit lung and breast tumors [25]. The aqueous insolubility and instability and thereby poor bioavailability prevent curcumin from successful clinical applications.

While an ongoing effort is to search stable curcumin analogs [26,27], curcumin delivery by nanocarriers has been recently

* Corresponding author at: Center for Bionanoengineering and State Key Lab of Chemical Engineering, Department of Chemical and Biological Engineering, Zhejiang University, Hangzhou 310027, China. Tel.: +86 571 8795 3993; fax: +1 307 7662501.
E-mail addresses: shenyq@zju.edu.cn, sheny@uwyo.edu (Y. Shen).

0142-9612/$ – see front matter © 2010 Elsevier Ltd. All rights reserved.
doi:10.1016/j.biomaterials.2010.06.007

explored to overcome these limitations. Curcumin loaded in liposomes [28–32] or nanoparticles [33–36], or conjugated to water-soluble PAMAM dendrimers [37] improved its water-solubility, stability and thus bioavailability. These systems, however, had disadvantages such as low loading efficiency and loading contents, varied loading contents from batch to batch. Curcumin was also conjugated to polyethylene glycol (PEG) through a liable urethane linkage to prepare water-soluble curcumin derivatives, but they were not stable and readily hydrolyzed even at neutral conditions (PBS, pH 7.4, $t_{1/2} = 60$ and 200 min, respectively) [38]. Even though the conjugates showed *in vitro* cytotoxicity against PC-3 pancreatic carcinoma cells, so far, no *in vivo* results were presented or followed this research.

Conjugation of drugs to the chain ends or side chains of water-soluble polymers, namely polymer-drug conjugates, is one of the general approaches to increase the drugs' water-solubility. However, this type conjugates can only carry several percent of hydrophobic drugs to make the conjugates water-soluble. Inspired by the bi-hydroxyl functionality of the curcumin molecule, we use curcumin as a comonomer to make curcumin-containing polymers (polycurcumins) by polycondensation polymerization. Curcumin units are incorporated in the polycurcumin backbones as a part of the carrier, leading to high curcumin-loading contents and efficiency without premature burst release. Other advantages of the polycurcumins include fixed curcumin loading contents, tailored water solubility, and adjustable hydrolysis kinetics. The polycurcumins may have a wide range of potential applications. Herein, we report the synthesis and characterization of the polycurcumins, and their *in vitro* and *in vivo* antitumor activities.

2. Materials and method

2.1. Materials

Tri(ethylene glycol) divinyl ether (98%), trifluoroacetic acid (99%), toluene 4-sulfonic acid (TSA 98%), cyclobutane-1,2,3,4-tetracarboxylic dianhydride (99%), *N*,*N*′-dicyclohexylcarbodiimide (DCC, 99%) 3,3′-dithiodipropionic acid, pyromellitic dianhydride (99%), 4-dimethylaminopyridine (DMAP, 99%), triethylamine (99%), polyethylene glycol (PEG) monomethyl ether (Mn = 1.1 kDa), 3-mercaptopropionic acid (99%), ethyl dichlorophosphate (98%) and diethylenetriaminepentaacetic dianhydride (99%) were purchased from Aldrich and used as received. Poly(ethylene glycol) (PEG, Mn = 200 or 400, Aldrich, 99%) was dried over calcium hydride. Curcumin (high purity, Axxora LLC) was further purified by repeated recrystallization in methanol. Permount was purchased from Sigma–Aldrich (St Louis, MO). 4′,6-Diamidino-2-phenylindole, dihydrochloride (DAPI) was purchased from Invitrogen Corporation (Carlsbad, CA). BrdU cell proliferation kit was purchased from Thermo Fisher Scientific Inc. (Waltham, MA). Primary antibodies were purchased from Santa Cruz Biotechnology Inc. (Santa Cruz, CA). Secondary antibodies were purchased from Jackson ImmunoResearch Laboratories Inc. (West Grove, PA).

2.2. Instrument

^{1}H NMR spectra were recorded on a Bruker Advance DRX-400 spectrometer. Deuterated acetone (acetone-d_6) or chloroform ($CDCl_3$) was dried over molecular sieve overnight before use. Chemical shift δ was given in ppm referenced to the internal standard tetramethylsilane (TMS, $\delta = 0$ ppm). The molecular weights of prepared curcumin polymers were determined by a Waters gel permeation chromatography (GPC) equipped with two 300 mm Waters Styragel solvent-saving columns (molecular weight ranges: 5×10^2–3×10^4, 5×10^3–6×10^5), a Waters 2414 refractive index detector, and a Precision 1102 light scattering detector. The eluent was THF at a flow rate of 0.3 mL/min with the column temperature of 30 °C. GPC data were recorded and processed using a Waters software package. HPLC analysis was performed on a Beckman System Gold equipped with a Jupiter Proteo 4 μ column (4.6×250 mm, Phenomenex, Torrance, CA) and a Beckman 166 UV detector. The mobile phase was 1:1 (v/v) acetonitrile/water containing 0.1% trifluoroacetic acid (TFA) with a flow rate of 1 mL/min for the measurements of free curcumin at detection wavelengths of 425 nm. The size of micelles or nanoparticles formed from polycurcumins was measured by a Nano-ZS Nanosizer (Malvern Instrument, UK) equipped with a 628 nm laser source.

2.3. Curcumin loading content and loading efficiency

The curcumin loading contents in polycurcumins were calculated from their NMR spectra. The drug loading efficiency was calculated based on the amount of incorporated curcumin *versus* the amount of curcumin initially added to the polymerization system using the following equations:

$$\text{Loading content}(\%) = \frac{\text{amount of curcumin incorporated into polycurcumin}}{\text{weight of the polycurcumin}} \times 100\%$$

$$\text{Drug loading efficiency}(\%) = \frac{\text{amount of curcumin incorporated into polycurcumin}}{\text{amount of curcumin intially added}} \times 100\%$$

2.4. Synthesis of the polycurcumins

In total, eight curcumin-containing polymers were synthesized (Scheme 1). The synthetic routes for these polycurcumins are given in Fig. S1 (Supporting Information). Typical synthesis procedures are as follows.

2.4.1. Synthesis of polycurcumin 1 (PCurc 1)

Curcumin (2.000 g) and pyromellitic dianhydride (1.183 g) were dissolved in 50 mL anhydrous dimethylsulfoxide (DMSO). After the mixture was stirred at 50 °C for 24 h, an excess of anhydrous tetrahydrofuran (THF) was added to precipitate the polymer product. This product (1.00 g) was redissolved in 40 mL anhydrous DMSO, followed by addition of 2.00 g of polyethylene glycol monomethyl ether (Mn = 1.1 k), 0.40 g of *N*,*N*′-dicyclohexylcarbodiimide (DCC), and 0.1 g of 4-dimethylaminopyridine (DMAP). This solution was stirred at room temperature for 24 h and an excess of anhydrous ether was then added to precipitate the final product, which was further purified by multiple precipitations from THF with anhydrous ether. The product was dried under vacuum to produce 2.2 g (yield 75%) of a deep yellow soft solid. ^{1}H NMR (acetone-d6, δ, ppm): 8.4 (br, 2H, $C_6H_2(COO)_4$), 7.6(br, m, 2H, $CH_b=CH_c$), 6.9–7.5 (br, m, 6.2H, C_6H_3), 6.7–6.8 (br, 2.1H, $CH_b=CH_c$), 6.0 (br, 1H, $CH_d=C-OH$), 4.2 (br, 2.1H, $COOCH_2CH_2O$), 3.9 (s, 6H, $CH_3OC_6H_3$), 3.5–3.7 (br, 118H, OCH_2CH_2O), 3.3 (s, 3.4 H, $CH_2CH_2OCH_3$). The NMR spectrum of PCurc 1 is supplied in Fig. S2 (Supporting Information). The integrations of the peaks from curcumin aromatic protons (6.9–7.5 ppm) and PEG ethylene protons (3.5–3.7 ppm) were used to calculate the curcumin content in the polymer. The calculated curcumin loading content was 20 wt.% and on average each repeating unit in the polymer chain was conjugated with 1.2 PEG chain. The free curcumin entrapped or adsorbed on PCurc 1 was determined by HPLC. Since almost all the curcumin monomer was incorporated into the polymer chain during the polycondensation reaction and the polymer was post-purified by multiple precipitations, the free curcumin in the polymer was quite low (0.4 wt.%) based on HPLC result.

2.4.2. Synthesis of polycurcumin 2 (PCurc 2)

Similarly, PCurc 2 was synthesized from diethylenetriaminepentaacetic dianhydride (1.940 g) with a yield of 75%. ^{1}H NMR (acetone-d6, δ, ppm): 7.6(d, 2H, $CH_b=CH_c$), 6.9–7.3 (m, 6.1H, C_6H_3), 6.7 (d, 2H, $CH_b=CH_c$), 6.0 (s, 1H, $CH_d=C-OH$), 4.2 (br, 2.1H, $COOCH_2CH_2O$), 3.9 (s, 6H, $CH_3OC_6H_3$), 3.5–3.7 (br, 128H, OCH_2CH_2O), 3.4 (s, 3.4 H, $CH_2CH_2OCH_3$), 2.6–2.7 (m, 8H, NCH_2CH_2N). The curcumin loading content was 18% and each unit was conjugated with 1.3 PEG chain on average. The free curcumin in the polymer was less than 0.2% as measured by HPLC.

2.4.3. Synthesis of polycurcumin 3 (PCurc 3)

PCurc 3 was synthesized similarly from 1.065 g of cyclobutane-1,2,3,4-tetracarboxylic dianhydride with a yield of 70%. ^{1}H NMR ($CDCl_3$, δ, ppm): 7.6(br, 2H, $CH_b=CH_c$), 6.9–7.2 (m, 6H, C_6H_3), 6.6 (br, 2H, $CH_b=CH_c$), 5.9 (br, 1H, $CH_d=C-OH$), 4.3 (br, 2H, $COOCH_2CH_2O$), 3.9 (s, 6H, $CH_3OC_6H_3$), 3.5–3.7 (br, 112H, OCH_2CH_2O), 3.4 (s, 3.7 H, $CH_2CH_2OCH_3$). The curcumin loading content was calculated to be 20% and each unit was conjugated with 1.1 PEG chain on average.

2.4.4. Synthesis of polycurcumin 4 (PCurc 4)

Curcumin (1.000 g), 3,3′-dithiodipropionic acid (0.571 g), DCC (1.15 g) and DMAP (0.1 g) were dissolved in 40 mL anhydrous THF, and reacted at room temperature for one day. PCurc 4 was isolated and purified as described above as a deep yellow solid (1.2 g, 81% yield). ^{1}H NMR (CDCl3, δ, ppm): 7.6 (d, 2H, $CH_b=CH_c$), 6.9–7.2 (m, 6H, C_6H_3), 6.6 (d, 2H, $CH_b=CH_c$) 5.9(s, 1H, $CH_d=C-OH$), 3.90(s, 6H, $CH_3OC_6H_3$), 2.9–3.2 (m, 8.4H, -CH_2CH_2–S–S–CH_2CH_2-). The calculated curcumin loading content was 66%.

2.4.5. Synthesis of polycurcumin 5 (PCurc 5)

Curcumin (0.876 g), 1.000 g of 3,3′-dithiodipropionic acid, 4.755 g PEG (Mn = 2 k), 2.0 g DCC, and 0.1 g of DMAP were dissolved in 80 mL anhydrous THF, and reacted at room temperature for one day. PCurc 5 as yellow powder was then isolated and purified as described above (5.2 g, 80% yield). ^{1}H NMR ($CDCl_3$, δ, ppm): 7.6 (br, 2H, $CH_b=CH_c$), 6.9–7.2 (br, 6H, C_6H_3), 6.6 (br, 2H, $CH_b=CH_c$) 5.8(br, 1H, $CH_d=C-OH$), 4.2 (s, 2H, $COOCH_2CH_2O$), 3.90(s, 6H, $CH_3OC_6H_3$), 3.5–3.7(br, 173H, OCH_2CH_2O), 2.9–3.2 (m, 17H, $-CH_2CH_2-S-S-CH_2CH_2-$). The curcumin loading

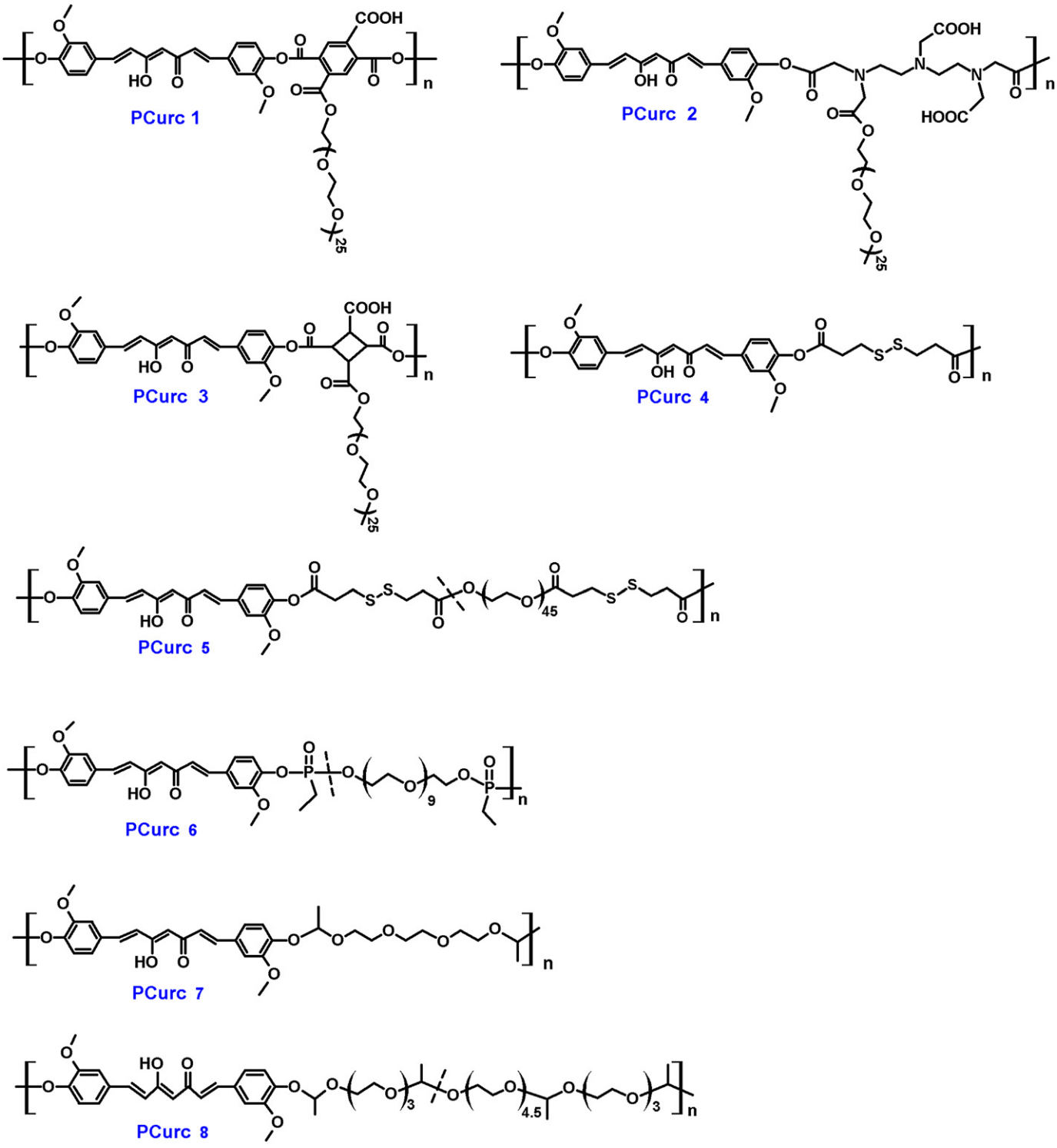

Scheme 1. Structures of the prepared polycurcumins.

content was calculated to be 14%. The free curcumin content in PCurc 5 was determined to be 0.3% by HPLC.

2.4.6. Synthesis of polycurcumin 6 (PCurc 6)

Curcumin (0.736 g), 0.8 g of PEG (Mn = 400), 0.652 g of ethyl dichlorophosphate, and 1.1 mL of triethylamine were dissolved in 40 mL anhydrous THF. The solution was stirred at 50 °C for 12 h, and then the THF was evaporated under vacuum. Chloroform (40 mL) was added to dissolve the polymer. The chloroform solution was washed with distilled water to remove the triethylamine salt. PCurc 7 was isolated and purified as described above as a yellow soft solid (1.8 g, yield 87%). ^{1}H NMR ($CDCl_3$, δ, ppm): 7.6 (br, 2H, $CH_b=CH_c$), 6.0–7.2 (br, 9H, C_6H_3, $CH_b=CH_c$ and $CH_d=C-OH$), 4.3 (br, 4.2H, $POOCH_2CH_2O$), 3.5–3.9 (br, 38H, OCH_2CH_2O), 1.3 (br, 7H, $P-CH_2CH_3$). The curcumin loading content was calculated to be 34%. The free curcumin in PCurc 6 determined by HPLC was about 0.4 wt.%.

2.4.7. Synthesis of polycurcumin 7 (PCurc 7)

Curcumin (1.800 g), 1.000 g of tri(ethylene glycol) divinyl ether, and 10 μg of toluene 4-sulfonic acid were dissolved in 40 mL anhydrous THF and reacted at 50 °C overnight. PCurc 7 was isolated and purified as described above as a yellow solid (2.4 g, 86% yield). ^{1}H NMR (acetone-d_6, δ, ppm): 7.6 (br, 2H, $CH_b=CH_c$), 6.8–7.4 (br,

8H, C_6H_3 & $CH_b=CH_c$), 4.7 (br, 2.1H, $(CH_3)CH$), 3.9 (br, 6H, $CH_3OC_6H_3$), 3.4–3.7 (br, 13H, OCH_2CH_2O), 1.2 (br, 6.7H, $(CH_3)CH$). The loading content was calculated to be 64%. The free curcumin in PCurc 7 was less than 0.1 wt.%.

2.4.8. Synthesis of polycurcumin 8 (PCurc 8)

Curcumin (1.10 g, 3.0 mmol), polyethylene glycol 200 (1.40 g, 7.0 mmol), tri (ethylene glycol) divinyl ether (2.12 g, 10.5 mmol), and 20 μg toluene 4-sulfonic acid were dissolved in 50 mL anhydrous THF and reacted at 50 °C overnight. PCurc 8 was isolated and purified as described above as a soft yellow solid (3.6 g, 78% yield). ^{1}H NMR ($CDCl_3$, δ, ppm): 7.3–7.7 (br, 2H, $CH_b=CH_c$), 6.3–7.2 (br, 8H, C_6H_3 & $CH_b=CH_c$), 4.80 (q, 6.2 H, $-(CH_3)CH-$), 3.5–3.8 (br, 97H, OCH_2CH_2O), 1.8 (d, 20H, $-(CH_3)CH-$). The curcumin loading content was calculated to be 21%. The free curcumin in PCurc 8 was 0.2 wt.%.

2.5. Hydrolysis of PCurc 8

The hydrolysis of PCurc 8 was conducted in pH 7.4 phosphate buffered saline (PBS) or pH 5.0 buffer to investigate the pH effect on hydrolysis kinetics. 10 mg of the purified PCurc 8 was dissolved in 5 mL buffer. The solution was kept at 37 °C under continuous stirring. At timed intervals, aliquots of the solution were withdrawn and diluted in THF for GPC measurement.

2.6. Cell line

The cell lines were purchased from American Type Culture Collection (ATCC). Cells were cultured in RPMI 1640 medium supplemented with 10% fetal bovine serum (HyClone, Logan, UT) at 37 °C in a humidified atmosphere of 5% CO2 (v/v). All experiments were performed on cells in the exponential growth phase.

2.7. Cytotoxicity assay

The cytotoxicity of polycurcumins was determined using the standard MTT cell proliferation kit (ATCC, Manassas, VA) according to the manufacturer's protocol. In brief, SKOV-3 ovarian cancer cells were seeded onto 96-well plates with a density of 15,000 cells per well and incubated at 37 °C in a humidified atmosphere of 95% air and 5% CO_2 for 16 h. The medium in each well was replaced with 200 μL of culture medium containing the treatments (polycurcumins) and cultured for 72 h. The medium in each well was then replaced with fresh medium and the cells were incubated for another 24 h. The incubation medium was then replaced with 100 μL of fresh medium and 10 μL of MTT reagent. After 6 h, 100 μL of detergent reagent was added to each well and incubated for 18 h at room temperature in the dark until all the crystals dissolved. The absorbance intensity at 570 nm was recorded on a Bio-Rad (model 550) microplate reader. Cell viability is defined as the percent live cells compared with untreated controls.

2.8. Cellular uptake of PCurc 8

SKOV-3 cells were seeded into glass bottom Petri dishes (MatTek, Ashland, MA) at 150,000 cells per plate in 2 mL of RPMI-1640 medium (Sigma–Aldrich) containing 10% FBS. The dishes were incubated for 24 h at 37 °C in a humidified atmosphere of 95% air and 5% CO_2 and then the medium was replaced with 2 mL of fresh medium containing desired concentrations of PCurc 8 and 50 nM lysotracker red (Molecular Probes, CA). After the dishes were cultured for 2 h or 24 h, 1 μM of nuclear dye DRAG5 (BioStatus, San Diego, CA) was added to the dishes and incubated for 5 min. The medium was then removed and washed with PBS and finally replaced with 2 mL PBS. Images were taken using a Leica TCS SP2 microscope. The Lysotracker red was excited with 543 nm laser and the emission wavelength was set from 580 to 620 nm and expressed as Red. PCurc 8 was observed using a 458 nm laser and the emission wavelength was read from 500 nm to 550 nm and expressed as green. The fluorescence emission and excitation spectra of PCurc 8 were shown in Figs. S3 and S4 (Supporting Information). The nuclear dye was excited with 633 nm laser and observed at wavelength from 680 nm to 720 nm and expressed as blue.

2.9. Analysis of apoptosis by Dapi staining

Dapi staining was used to detect apoptosis *in vitro*. 70,000 cells were cultured in 12-well plates with coverslips in each well. After treatment with 40, 20 and 10 μg/mL of PCurc 8 for 72 h, the treatment was removed and 1 mL fixative solution was added into each well for 15 min incubation. Fixative solution in each well was replaced by 1 mL Dapi solution (the final concentration 10 μg/mL) and incubated for 15 min. Then Dapi staining solution was removed and the cells were washed by PBS twice before coverslips were mounted on the slides by permount. To measure the effect of caspase-3 inhibitor (Z-DEVD-FMK) on the PCurc 8 induced apoptosis, 100 μM of Z-DEVD-FMK was add 2 h prior to the treatment and co-incubated with PCurc 8 for 72 h. The fluorescence of Dapi at 461 nm excited at 350 nm was observed under Olympus BX 51 microscope.

2.10. BrdU incorporation and immunofluorescence assay

DNA synthesis was determined by measuring BrdU incorporation into DNA as the instruction suggested. Briefly, cells were cultured in 24-well plate with coverslips for 24 h with complete medium. Complete medium was replaced with FBS-free medium for another 12 h. PCurc 8 solution was added into each well for 24 h incubation. BrdU solution was incubated with cells for 30 min before fixation and blocking. Then primary antibody and DyLight 549 conjugated secondary antibody were used to label the BrdU in the cell nucleus. Nikon TE300 microscope was used to observe the fluorescence at 617 nm excited at 555 nm.

2.11. Western analysis for proteins

Cells were initially seeded at a density of 1×10^6 in 75 mm^2 flasks. After treatment at the indicated concentrations of PCurc 8 for 24 h, cells were gently scraped from the dishes and collected. The proteins of SKOV-3 cells were extracted in Laemli buffer and the protein concentrations were measured by A280 using Nanodrop ND-1000 (Thermo Scientific, Waltham, MA). The total proteins were fractionated on 12% Tris-Glycine precast gels, transferred to nitrocellulose membrane (Life Science Product Inc., Frederick, CO), and probed with primary antibodies and HRP-labeled secondary antibodies. Proteins were visualized using Supersignal West Pico chemiluminescent substrate detection reagents (Thermo scientific, Waltham, MA).

2.12. Animals

Athymic nude mice (BALB/c nu/nu, Charles River) were maintained in compliance with the policy on animal care expressed in the National Research Council guidelines (NRC 1985) and all experiments were approved and supervised by the Institutional Animal Care and Use Committee (IACUC) at the University of Wyoming. Mice were maintained in a pathogen-free environment under controlled temperature (24 °C) and lighting (12L:12D) conditions. Autoclaved rodent chow and sterilized water were supplied *ad libitum*.

2.13. Antitumor activity against SKOV-3 human ovarian carcinoma xenografts

SKOV-3 cells (5×10^6 suspended in 2.0 mL PBS) were injected into the abdominal cavity of mature nude mice (12–16 weeks). The mice were randomly divided into a treatment group and a control group ($n = 6$) at five weeks post-inoculation (when tumors along the mesentery were well established). Curcumin group was not included because it is practically water-insoluble and unstable in PBS. The treatment group was injected intravenously (i.v.) through the tail vain with PCurc 8 in 0.1 mL PBS at 100 mg/kg and the control group was injected with 0.1 mL PBS. The mice were sacrificed and dissected 48 h after the injection. All tumor tissues were collected and the total tumor weight of each mouse was measured. The difference in tumor weight between the control group and treatment group was used as an overall mark of antitumor activity of the PCurc 8 against the SKOV-3 xenografts.

2.14. Statistics analysis

Assignments to treatments were made at random. Treatment comparisons were made by analysis of variance and protected least significant difference or Student's *t*-test. Contrasts were considered different at $P < 0.05$. Data are presented as means ± standard errors.

3. Results

3.1. Syntheses and characterizations of the polycurcumins

Curcumin as a monomer was easily polymerized with diacid, dianhydride or divinyl ether comonomers to high molecular weight polymers (Fig. S1 in Supporting Information). Table 1 lists the molecular weights of all polycurcumins prepared. The molecular weights of the polycurcumins ranged from 10^4 to 10^5 with polydispersities between 1.4 and 2.6, which is typical for polymers made from condensation polymerization. The loading contents calculated according to the feeding ratios were very close to the values determined from the polymers' NMR spectra. Therefore, the loading efficiencies were very close to 100%.

Because of the strong hydrophobicity of curcumin, the polycurcumins directly made from curcumin with diacids or dianhydrides were water insoluble (e.g. PCurc 4 and 7). Therefore, short PEG chains were either introduced as side chains (PCurc 1–3) or used as a comonomer incorporated into the backbones (PCurc 5, 6 and 8) to increase their water solubilities. The solubility of the

Table 1
The molecular weight, solubility, curcumin loading content and efficiency of the prepared polycurcumins.

Entry	Mn ($x10^4$)	PDI	Solubility in water*	Theoretical loading content	Measured Loading Content	Loading efficiency
PCurc 1	2.95	2.4	S	21.2%	20%	94%
PCurc 2	1.38	2.6	S	17.1%	18%	100%
PCurc 3	1.15	2.1	S	22.0%	20%	91%
PCurc 4	6.13	1.5	I	67.9%	66%	97%
PCurc 5	1.73	1.9	S	13.4%	14%	100%
PCurc 6	1.28	1.8	PS	36.0%	34%	94%
PCurc 7	2.14	2.2	I	64.3%	64%	99%
PCurc 8	4.50	1.4	S	23.8%	21%	88%

* S: Soluble; PS: Partially soluble; I: Insoluble.

resulting polycurcumin could be tailored by the curcumin/PEG ratio and/or the PEG chain length. Incorporation of more or longer PEG chains increased the polycurcumin's water-solubility but lowered its curcumin loading content (Table 1).

PCurcs 1–3 had hydrophobic backbones grafted with hydrophilic PEG side chains. They dissolved in water but formed core-shell structured micelles or nanoparticles with average diameters in the range of 100–400 nm (Fig. S5 in Supporting Information), which could be used as carriers for other drugs. PCurc 5 and 8 with hydrophilic PEG in their backbones did not form micelles or nanoparticles under the experimental conditions, as evidenced from Fig. S6 in Supporting Information. PCurcs 4, 6, and 7 were water-insoluble.

3.2. *In vitro cytotoxicity of polycurcumins to SKOV-3 cancer cell lines*

SKOV-3 ovarian cancer cells of human origin were first used to screen the cytotoxicity of polycurcumins by a standard MTT assay. PCurc 4, 6 and 7 were not tested because they were water insoluble or poorly soluble. The commoners such as 3,3′-dithiodipropionic acid, pyromellitic dianhydride, tri(ethylene glycol) divinyl ether and PEG were used as controls. These controls showed no significant cytotoxicity against SKOV-3 cells, which means that the cytotoxicity of the polycurcumins solely came from curcumin. Curcumin was used as a control by dissolving it in DMSO at a concentration of 5 mg/mL, followed by dilution in medium to the needed doses. The MTT assay results are shown in Fig. 1. The IC_{50} values were calculated from their dose response curves and the results are summarized in Table 2. The IC_{50} value in terms of the polycurcumin dose (IC_{50-P}) and that in terms of curcumin-equivalent dose (IC_{50-C}) is exchangeable using the equation: $IC_{50-C} = IC_{50-P} \times$ loading content.

Table 2 shows that the PCurc 2, 3 and 5 had lower cytotoxicity to SKOV-3 cells than curcumin while PCurc 1 had similar cytotoxicity to curcumin. PCurc 8 had the highest cytotoxicity with a much lower IC_{50} (1.2 μg/mL) than free curcumin.

The cytotoxicity of PCurc 8 to other cancer cell lines such as MCF-7 breast carcinoma and OVCAR-3 ovarian carcinoma was subsequently assessed. Fig. 2 shows the dose- response curves of the PCurc 8 to the cells. For comparison, the curves of curcumin and PCurc 8 to SKOV-3 were also included. Obviously, PCurc 8 was highly cytotoxic to not only SKOV-3 cells but also OVCAR-3 and

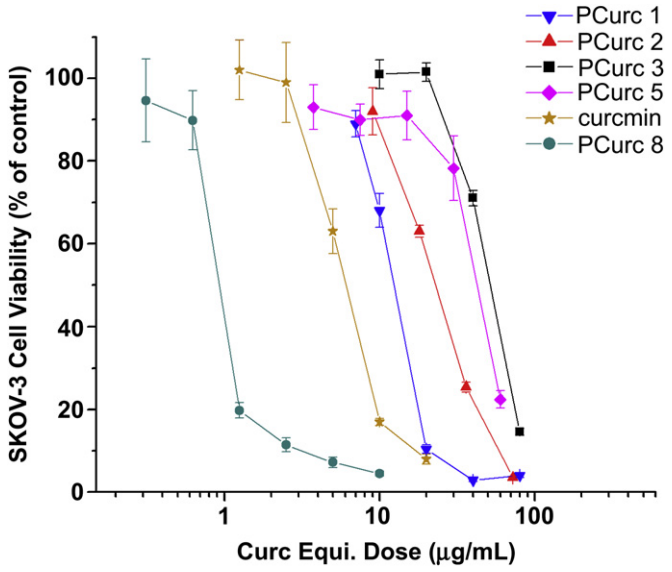

Fig. 1. Cytotoxicities of polycurcumins and curcumin to SKOV-3 cancer cells. Cells were treated with polycurcumins for 72 h followed by 24 h incubation in free medium.

MCF-7 cancer cells. The IC_{50} value in terms of the curcumin-equivalent dose was calculated to be 1.4 μg/mL (3.8 μM) to MCF-7 cells and 0.4 μg/mL (1.1 μM) to OVCAR-3 cells. Therefore, PCurc 8 was selected to further evaluate its hydrolysis, cellular uptake, cell cycle arrest ability, and *in vivo* antitumor activity.

3.3. *The hydrolysis of PCurc 8*

Acetal bonds can easily hydrolyze at acidic pH producing diols and acetaldehyde [39]. The hydrolysis of PCurc 8 should produce oligomers and finally curcumin (Scheme 2). GPC curves of the hydrolyzed PCurc 8 at different pH values are shown in Fig. 3. Obviously, the hydrolysis at pH 5.0 was fast. The polymer quickly degraded from high molecular weight (4.5×10^4) to oligomers (3.8×10^3) in 8 h. After 16 h, almost all PCurc 8 hydrolyzed to small molecules. In contrast, its hydrolysis at pH 7.4 was very slow. The major peak of PCurc 8 didn't shift to low molecular weight even after 48 h. Thus, PCurc 8 was expected to be stable at neutral conditions such as in the blood circulation and normal tissues.

3.4. *Cellular uptake of PCurc 8 by SKOV-3 cells*

Cellular uptake of PCurc 8 was first probed using confocal fluorescent microscopy (Fig. 4). PCurc 8 had a weak green fluorescence (Fig. S3) and thus the fluorescence was used to monitor the intracellular PCurc 8. A high dose, 25 μg/mL, was used because the fluorescence was weak. PCurc 8 was quickly endocytosized into the cells (green spot). Overlap of the image with the one taken from the Lysotracker Red channel produced yellow spots, indicating that PCurc 8 was all in lysosomes within the 2 h incubation (Fig. 4 A–C). Even after 24 h incubation, the PCurc 8 still stayed in the lysosomes

Table 2
The IC_{50} values to SKOV-3 cell line of polycurcumins (IC_{50-P}) and their curcumin-equivalent doses (IC_{50-C}) calculated using their loading contents (L.C.).

Entry	PCurc 1	PCurc 2	PCurc 3	PCurc 5	PCurc 8	Curcumin
IC_{50-P} (μg/mL)	63.5	123.8	277.0	301.3	5.7	/
L. C. (%)	20	18	20	15	21	/
IC_{50-C} (μg/mL)	12.7	22.3	55.4	45.2	1.2	7.8

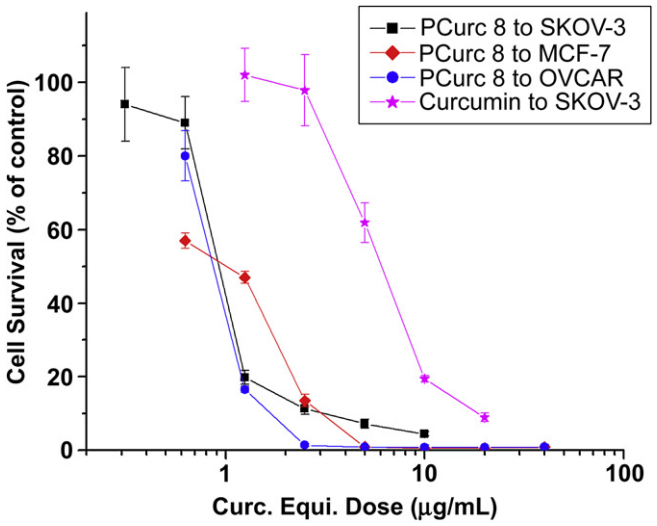

Fig. 2. Cytotoxicities of PCurc 8 to SKOV-3, OVCAR-3 and MCF-7 cancer cell lines. Cells were treated with PCurc 8 for 72 h followed by 24 h incubation in free medium.

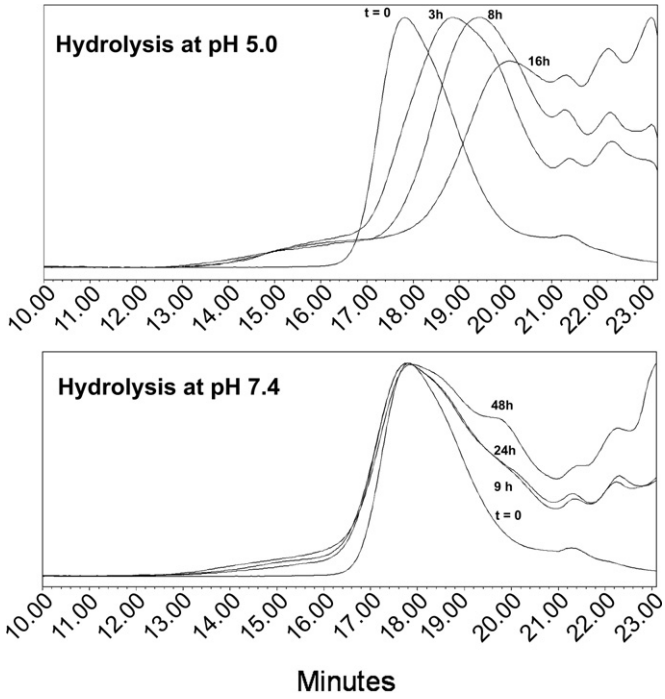

Fig. 3. GPC profiles of hydrolysis of PCurc 8.

and no PCurc 8 was in the nucleus (Fig. 4 D–F). In contrast, curcumin was reported to primarily localize in the cell membrane and nucleus due to its lipophilic properties [40]. The altered intracellular distribution of PCurc 8 indicated the high molecular weight polymer was internalized mainly by endocytosis.

3.5. Retardation of cell cycle by PCurc 8

Curcumin was found to induce cell cycle arrest by down-regulating cyclin D1 expression [41,42]. The cell cycle arrest ability of PCurc 8 was examined by immunofluorescence analysis (Fig. 5). BrdU was labeled with DyLight 549 (pseudo-colored as red), and the cell nucleus was stained by Dapi (pseudo-colored as blue). The untreated cells had red BrdU fluorescence (Fig. 5A) and 28% of them counted randomly on the slides expressed BrdU fluorescence. However, PCurc 8 treated cells had no DyLight labeled BrdU fluorescence (Fig. 5 D). Since BrdU can only be incorporated into the newly synthesized DNA of replicating cells already in S phase [43], this result implies that PCurc 8 induced cell cycle arrest at G_0/G_1 phase rather than G_2/M phase.

To confirm the result from BrdU detection, the proteins which control the progression of cells from G_0/G_1 phase into S phase were examined by western-blot. Cyclin D and cyclin dependent kinases CDK 4 and CDK 6 are required in the passage through G_1 phase [44,45]. The formation of Cyclin D1/CDK4 and Cyclin D1/CDK6 complex is the key factor that regulates the cell cycles from G_1 phase to S phase. As shown in Fig. 6, CDK4, and CDK6 were significantly down-regulated after treatment with PCurc 8, indicating that the SKOV-3 cells were retarded at G_0/G_1 or G_1 phase before entering into S phase.

3.6. Apoptosis induced by PCurc 8

After confirmed the retardation of cell cycle by PCurc 8, the cell apoptosis induced by the cell arrest was also investigated by Dapi staining. Fig. 7 shows the results of SKOV-3 cells treated by PCurc 8 at dose of 20 μg/mL and 40 μg/mL for 72 h. Clearly, significant apoptosis was observed and only a few cells survived after 72 h treatment at both doses. Small apoptotic bodies could also be observed under microscopy. To examine the role of caspase-3 in PCurc 8-induced apoptosis, Western-blot was used to determine the protein expression of procaspase-3 (Fig. 6). Obviously, the procaspase-3 was down-regulated by PCurc 8 in a dose-dependent fashion, implying that PCurc 8 promoted the conversion of procaspase-3 to caspase-3 and thus triggered the apoptotic process. Addition of caspase-3 selective inhibitor (Z-DEVD-FMK) was used to determine the effect of caspase-3 on PCurc 8-induced apoptosis. By blocking caspase-3 activity, significantly more cells survived at a PCurc 8 dose of 20 μg/mL (Fig. 7D vs. Fig. 7B). But at 40 μg/mL of PCurc, the same dose of Z-DEVD-FMK did not block the apoptosis (Fig. 7E vs. Fig. 7C). This result indicates PCurc 8-induced apoptosis

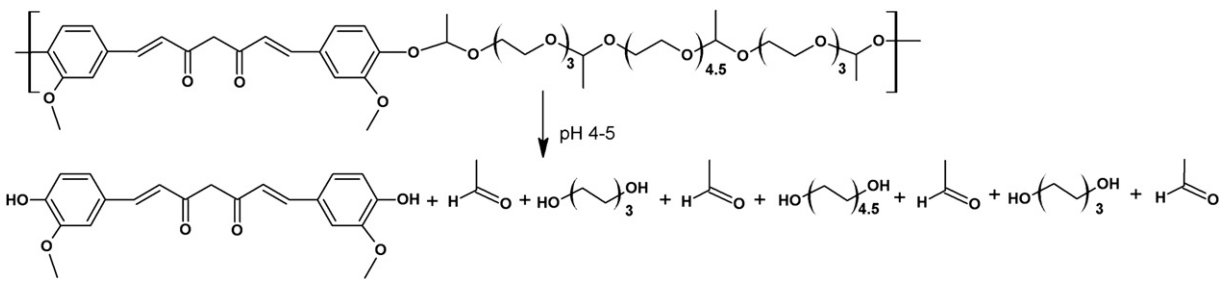

Scheme 2. Acid catalyzed hydrolysis of PCurc 8.

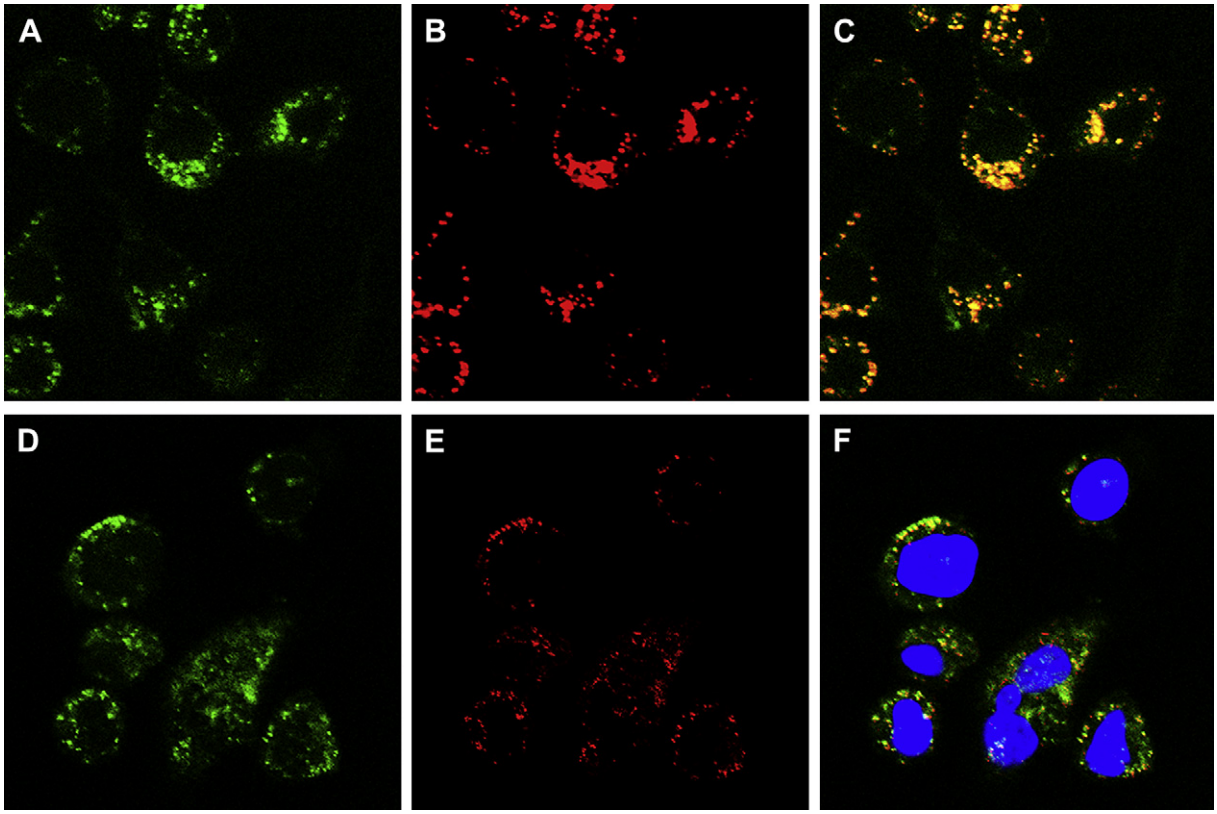

Fig. 4. Intracellular distribution of PCurc 8 observed by confocal microscopy. SKOV-3 cells were treated PCurc 8 at 25 μg/mL for 2 h (A–C) and 24 h (D–F). Images were taken from the PCurc 8 channel (Left column, green) and the Lysotracker channel (middle column, red), and overlapped of two channels (the right column). The image F is also overlapped with the nuclear dye channel (Blue).

may be executed through both a caspase-dependent pathway and a caspase-independent pathway, as natural curcumin did [41].

3.7. *In vivo antitumor activity of PCurc 8 to SKOV-3 xenografts*

The *in vivo* antitumor activity of PCurc 8 was preliminarily evaluated using SKOV-3 xenografts animal model. The athymic nude mice burdened with human SKOV-3 ovarian intraperitoneal tumors were treated with a single i.v. injection of PCurc 8 at a 100 mg/kg dose (21 mg/kg curcumin-equivalent dose) or PBS (control) through the mice tail veins. Curcumin group was not investigated because curcumin is practically insoluble in PBS, and could not be i.v. administered under the identical conditions to PCurc 8 administration. Significant antitumor activity was observed for PCurc 8 against SKOV-3 xenograft (Fig. S7 in Supporting Information). The control group had an average tumor burden of 1.57 g while the PCurc 8-treated group had 0.49 g, a 68% decrease in tumor growth compared to the control group, suggesting a remarkable tumor growth inhibition ability of PCurc 8.

4. Discussion

It is widely accepted that the drug conjugated to a carrier must be liberated to elicit its pharmaceutical actions [46]. Unlike normal tissues, solid tumor tissues usually have an acidic extracellular environment with an averaged pH of 6.81 ± 0.09 and the lowest value of 5.55 [47]. Furthermore, water-soluble polymers and their conjugates have been shown to be endocytosized to lysosomes [46], where the pH is even more acidic (pH 4–5) [48]. Therefore, all the polycurcumins were designed to be stable under the neutral physiological conditions but hydrolyzable under weakly acidic conditions. PCurc 1–6 were made using hydrolyzable ester bonds, which are relatively stable at the physiological pH (7.4) but hydrolyzable at acidic pH. In PCurc 4 and 5, disulfide bonds were further introduced for intracellular glutathione (GSH)-induced cleavage of the backbones. GSH is a thiol-containing tripeptide that can reduce and break disulfide bond. The glutathione concentration is very low in blood (in micromolar range) but high enough in cytosol (in millimolar range) to cause the scission of disulfide bond [49]. Thus, the high concentration of intracellular GSH is expected to cleave the disulfide bonds and accelerate the hydrolysis of the ester bonds in PCurc 4 and 5. PCurc 7 and 8 used acetal bonds to connect curcumin. Polyacetals are also stable at the neutral and basic conditions but hydrolyzable in acidic conditions, releasing diols (curcumin in PCurc 8) and acetaldehyde [39] (Scheme 2).

Due to the high hydrophobicity of curcumin, the polymers from the direct condensation of curcumin with either dianhydride, diacid or divinyl ether compounds were all water-insoluble. Therefore, short PEG chains were either grafted to the backbones (PCurc 1–3) or as a comonomer during the condensation polymerization (PCurc 5, 6 & 8) to increase their water-solubilities. The introduction of PEG chains decreased the curcumin-loading content, and at 25 wt.% or lower curcumin-contents the resulting polymers were water-soluble.

The high molecular weights of the polycurcumins indicated that the condensation reactions had high monomer conversions (>95%, $X_n = 1/(1-p)$, where X_n is the polymerization degree and p is the monomer conversion). Therefore, the loading efficiency of curcumin should be close to 100% since almost all curcumin was incorporated into polycurcumins, as shown in Table 1. Thus, the polycurcumins

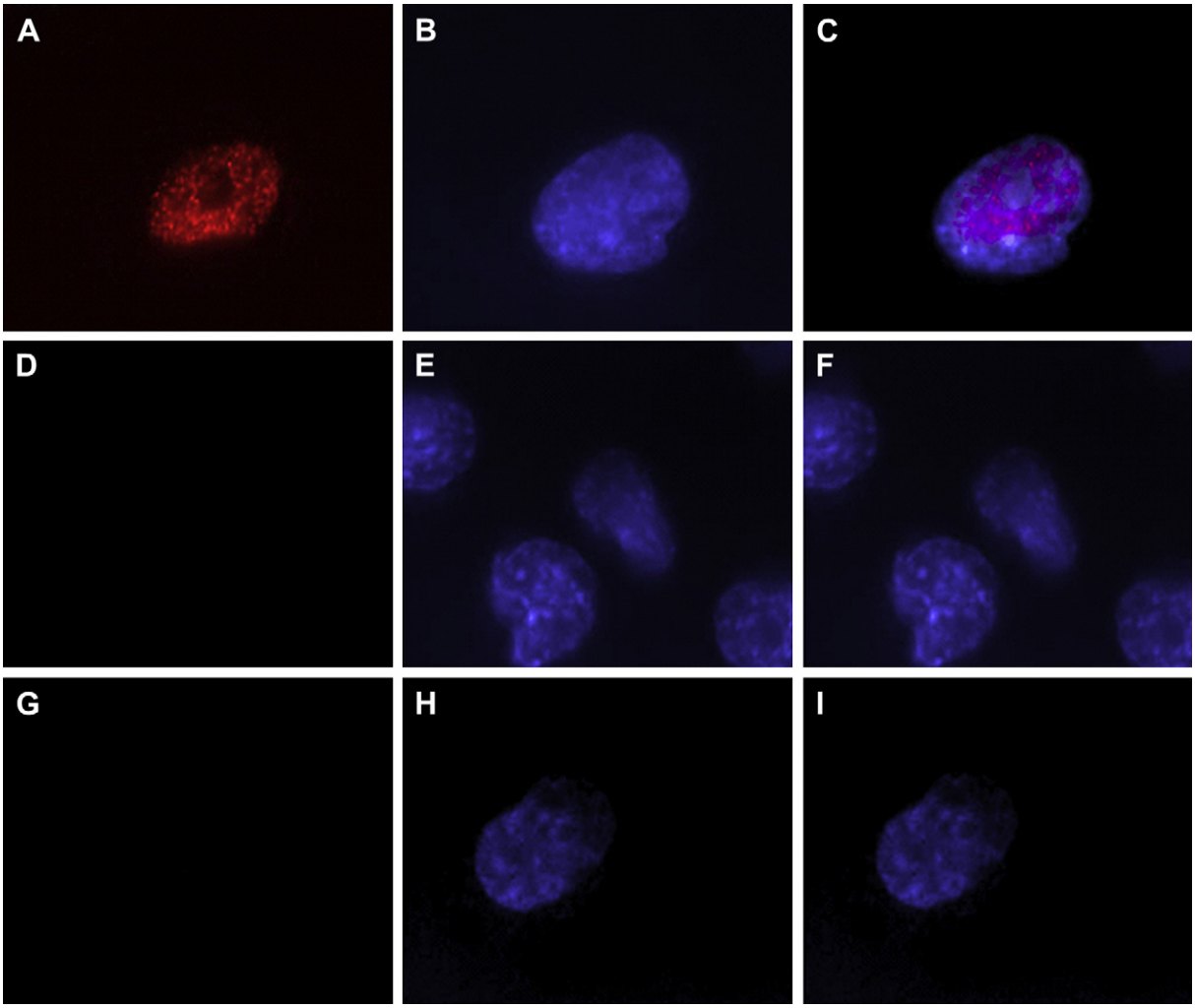

Fig. 5. Analysis of PCurc 8-induced cell cycles of SKOV-3 cells by immunofluorescence assay. The SKOV-3 cells were untreated (upper row), or treated with 20 μg/mL PCurc-8 (middle row), or 40 μg/mL PCurc-8 (lower row) for 24 h, followed by addition of BrdU, monoclonal primary antibody, and DyLight 549-conjugated secondary antibody. Images were taken from the BrdU immunofluorescence channel (A, D, G), DAPI channel (B, E, H), and overlapped the two channels (C, F, I).

can be considered as backbone-type polymer-drug conjugates, a new form of drug conjugate. In addition to the high loading efficiencies, their compositions will not vary from batch-to-batch and thus have fixed loading contents once the polymerization conditions and the comonomer ratios are kept constant. The water-solubility, and hydrolysis rate are easily tunable to meet different applications by changing the feeding ratio of curcumin and co-monomers.

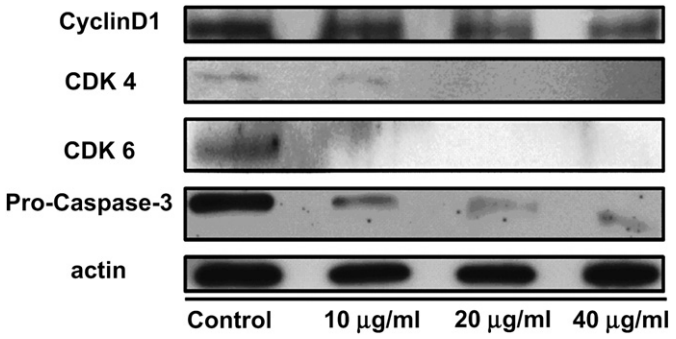

Fig. 6. Protein expression detected by Western Blot of the SKOV-3 cells treated with PCurc 8. Cells were treated with 10, 20 and 40 μg/mL of PCurc 8 for 24 h. Equal amount of the proteins were fractionated on SDS-polyacrylamide gels and transferred to nitrocellulose membrane, followed by immunobloting with anti-Cyclin D1, CDK4, CDK6 and procaspase-3 antibodies. Immunoblotting of β-actin was shown to demonstrate loading equivalency.

The cytotoxicity of the polycurcumins was first tested to screen out the one most cytotoxic to cancer cells. The polyester-based PCurc 1–6 had lower cytotoxicity than pristine curcumin, probably because their hydrolysis was not sufficiently fast to release active curcumin. The polyacetal-based PCurc 8 was more cytotoxic than curcumin. Its IC_{50} was about one-sixth of that of curcumin (Fig. 1). Very importantly, PCurc 8 also had high cytotoxicity to other cancer cell lines (Fig. 2). The high cytotoxicity of PCurc 8 may be due to its fast hydrolysis at the lysosomal pH (Fig. 3) and the improved stability in neutral conditions. Curcumin was insoluble in water and rapidly degraded at neutral or alkaline conditions with an half life ($t_{½}$) time less than 10 min in PBS at pH 7.2 [24], but curcumin with its two hydroxyl group capped became much more stable [37,38]. PCurc 8 was fast taken up into cancer cells and selectively localized in lysosomes (Fig. 4), ensuring that PCurc 8 quickly hydrolyzed at the acidic lysosomal pH (4–5) and released curcumin. Curcumin is stable in the acidic condition [24] (lysosomes). Once it diffused out into the cytosol, it could immediately exert its biological actions.

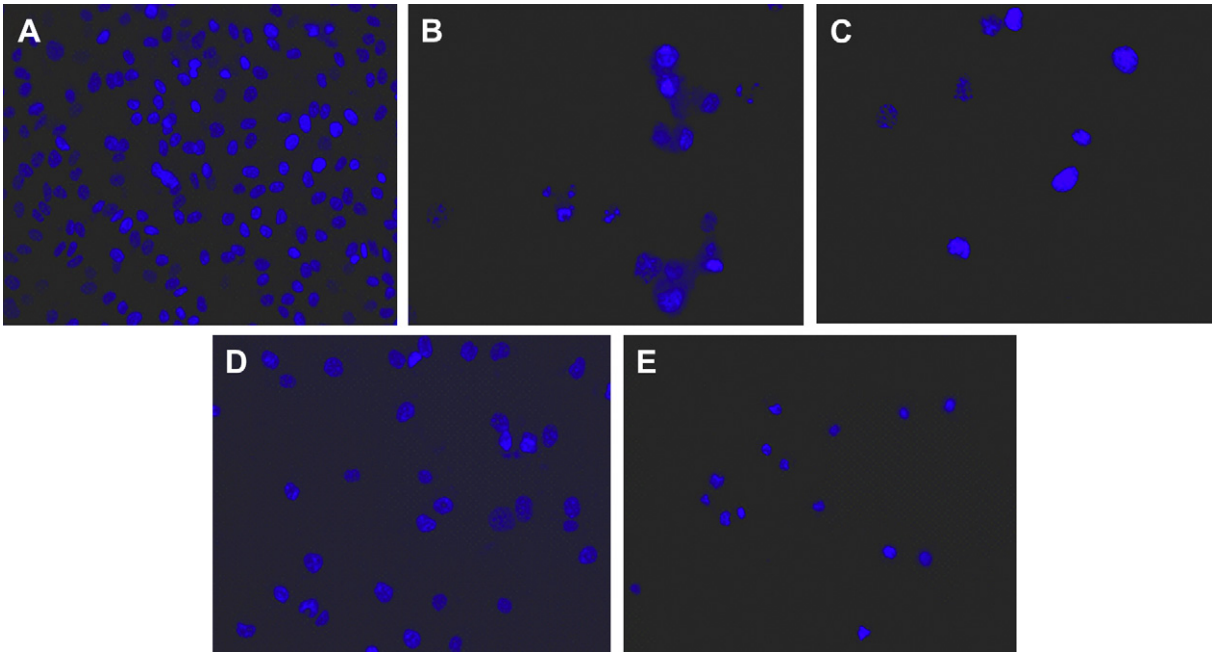

Fig. 7. PCurc 8-induced apoptosis of SKOV-3 cells detected by Dapi staining. Cells were untreated (control, A), or treated for 72 h with 20 μg/mL PCurc 8 (B), 40 μg/mL PCurc 8 (C), 20 μg/mL of PCurc 8 with 100 μM Z-DEVD-FMK inhibitor (D), and 40 μg/mL PCurc 8 with 100 μM Z-DEVD-FMK inhibitor (E). In the Z-DEVD-FMK groups, the inhibitor was added 2 h prior to the treatment.

As curcumin was reported to have many pathways inducing cell apoptosis, only selected ones were examined to preliminarily investigate the mechanism of PCurc 8-induced apoptosis of SKOV-3 cells. As shown in Fig. 7, the pretreatment of Z-DEVD-FMK significantly blocked PCurc 8-induced apoptosis (Fig. 7B *versus* 7D) at low doses, suggesting that caspase-3 activation may play important role in mediating PCurc 8-induced apoptosis. Western-blot result showed that PCurc 8 significantly down-regulated the protein level of pro-caspase-3 in SKOV-3 cells in a dose-dependent fashion (Fig. 6 panel 4), which clearly indicated that caspase-3 activation was involved in PCurc 8-induced cell apoptosis. The SKOV-3 cells treated with PCurc 8 showed no BrdU fluorescence (Fig. 5D and G), implying that PCurc 8 significantly suppressed DNA synthesis and subsequently inhibited cell proliferation. The CDK 4 and CDK 6 are known to bind to Cyclin D1 to form a pRB kinase as a key regulator in cell cycle transitions from the G_1/G_0- to S-phase and for DNA replication [44,45]. The significant down-regulation of CDK4 and CDK6 by PCurc 8 provided additional evidence to the inhibitory effect of PCurc 8 on DNA synthesis and indicated that the SKOV-3 cells were arrested at the G_0/G_1 or G_1 phase before entering into the S phase. This is different from pristine curcumin. Curcumin was found to induce cell cycle arrest at G_2/M phase in A-549 lung cancer cells and reversibly inhibit normal mammary epithelial cell cycle at G_0 phase by down-regulating cyclin D1 expression [41,42].

Curcumin and its derivatives are found effective *in vitro* tests but mostly ineffective *in vivo* anticancer tests [22,23]. The *in vivo* antitumor activity of PCurc 8 was preliminarily examined. Very interestingly, PCurc 8 significantly reduced the i.p. SKOV-3 cell tumor growth with single i.v. injection. The drastic tumor suppression ability of PCurc 8 is even comparable to those of some targeted anticancer drugs such as camptothecin (CPT) [50,51]. The detailed mechanism of the vigorous antitumor activity of PCurc 8 is still unknown at present but may result from its stability, water solubility, and thus better bioavailability. Unlike curcumin, PCurc 8 is water-soluble (solubility $>$ 30 mg/mL), and stable in physiological conditions. Its high molecular weight endows it a longer blood circulation time and therefore the PCurc 8 has better chance to be passively accumulated in tumor tissues via their enhanced permeability and retention effects [52]. The detailed *in vivo* study, the antitumor activity to other human origin carcinomas and the tumor prevention ability of PCurc 8 are currently under investigation.

5. Conclusions

Curcumin is polymerized by condensation reaction to form a series of backbone-type curcumin-derived high polymers. The polymers have tailored curcumin-loading contents and water-solubility. Of them, the PCurc 8 was water soluble, i.v. injectable, and stable in physiological conditions. MTT assay results showed that PCurc 8 was more cytotoxic to SKOV-3, MCF-7, and OVCAR-3 cancer cell lines than curcumin. The PCurc 8 arrested the SKOV-3 cell cycle at the G_0/G_1 phase *in vitro* and induced cell apoptosis partially through caspase-3 dependent pathway. In vivo, the polymer showed remarkable antitumor activity in a SKOV-3 i.p. tumor-xenograft animal model. Thus, the stable and water-soluble PCurc 8 is i.v. injectable and is greatly advantageous over water-insoluble curcumin, which is generally administrated either oral gavage or intraperitoneal (i.p.) injection [22] or intravenously (i.v.) administration of its glycerolformal solution [53]. This polymer is merited for further study as a new polymer-drug conjugate for cancer chemotherapy.

Acknowledgements

The authors thank the National Fund for Distinguished Young Scholars (50888001) and the National Basic Research Program (973 Program, 2009CB526403) of China, and the Department of Defense (BC083821) of USA for financial supports of this research.

Appendix. Supplementary data

The supplementary data associated with this article can be found in the on-line version at doi:10.1016/j.biomaterials.2010.06.007.

Appendix

Figures with essential color discrimination. Figs. 1, 2, 4, 5 and 7 in this article are difficult to interpret in black and white. The full color images can be found in the on-line version, at doi:10.1016/j.biomaterials.2010.06.007.

References

[1] Aggarwal BB, Surh YH, Shishodia S, editors. The molecular targets and therapeutics of curcumin in health and disease. Springer; 2007.
[2] Strimpakos AS, Sharma RA. Curcumin: preventive and therapeutic properties in laboratory studies and clinical trials. Antioxid Redox Signal 2008;10(3):511–46.
[3] Aggarwal BB, Harikumar KB. Potential therapeutic effects of curcumin, the anti-inflammatory agent, against neurodegenerative, cardiovascular, pulmonary, metabolic, autoimmune, and neoplastic diseases. Int J Biochem Cell Biol 2009;41(1):40–59.
[4] Somparn P, Phisalaphong C, Nakornchai S, Unchern S, Morales NP. Comparative antioxidant activities of curcumin and its demethoxy and hydrogenated derivatives. Biol Pharm Bull 2007;30(1):74–8.
[5] Menon VP, Sudheer AR. Antioxidant and anti-inflammatory properties of curcumin. Adv Exp Med Biol 2007;595:105–25.
[6] Chen D, Nie M, Fan MW, Bian Z. Anti-inflammatory activity of curcumin in macrophages stimulated by lipopolysaccharides from *Porphyromonas gingivalis*. Pharmacology 2008;82(4):264–9.
[7] Bar-Sela G, Epelbaum R, Schaffer M. Curcumin as an anti-cancer agent: review of the gap between basic and clinical applications. Curr Med Chem 2010;17(3):190–7.
[8] Reuter S, Eifes S, Dicato M, Aggarwal BB, Diederich M. Modulation of anti-apoptotic and survival pathways by curcumin as a strategy to induce apoptosis in cancer cells. Biochem Pharmacol 2008;76(11):1340–51.
[9] Singh S, Aggarwa BB. Activation of transcription factor NF-kB is suppressed by curcumin (diferulolylmethane). J Biol Chem 1995;270(42):24995–5000.
[10] Kunnumakkara AB, Anand P, Aggarwal BB. Curcumin inhibits proliferation, invasion, angiogenesis and metastasis of different cancers through interaction with multiple cell signaling proteins. Cancer Lett 2008;269(2):199–225.
[11] Farombi EO, Shrotriy S, Surh Y-J. Kolaviron inhibits dimethyl nitrosamine-induced liver injury by suppressing COX-2 and iNOS expression via NF-κB and AP-1. Life Sci 2009;84(5–6):149–55.
[12] Liu JY, Lin SJ, Lin JK. Inhibitory effects of curcumin on protein kinase C activity induced by 12-O-tetradecanoylphorbol-13-acetate in NIH 3T3 cells. Carcinogenesis 1993;14(5):857–61.
[13] Shukla S, Zaher H, Hartz A, Bauer B, Ware JA, Ambudkar SV. Curcumin inhibits the activity of ABCG2/BCRP1, a multidrug resistance-linked ABC drug transporter in mice. Pharm Res 2008;26(2):480–7.
[14] Zhang W, Tan TMC, Lim L-Y. Impact of curcumin-induced changes in P-glycoprotein and CYP3A expression on the pharmacokinetics of peroral celiprolol and midazolam in rats. Drug Metab Dispos 2006;35(1):110–5.
[15] Sandur SK, Pandey MK, Sung B, Ahn KS, Murakami A, Sethi G, et al. Curcumin, demethoxycurcumin, bisdemethoxycurcumin, tetrahydrocurcumin and turmerones differentially regulate anti-inflammatory and anti-proliferative responses through a ROS-independent mechanism. Carcinogenesis 2007;28(8):1765–73.
[16] Song G, Mao YB, Cai QF, Yao LM, Ouyang GL, Bao SD. Curcumin induces human HT-29 colon adenocarcinoma cell apoptosis by activating p53 and regulating apoptosis-related protein expression. Braz J Med Biol Res 2005;38(12):1791–8.
[17] Li L, Braiteh FS, Kurzrock R. Liposome-encapsulated curcumin: in vitro and in vivo effects on proliferation, apoptosis, signaling, and angiogenesis. Cancer 2005;104(6):1322–31.
[18] Purkayastha S, Berlinerb A, Fernandoa SS, Ranasinghe B, Ray I, Tariq H, et al. Curcumin blocks brain tumor formation. Brain Res 2009;1266(17):130–8.
[19] Lin YG, Kunnumakkara AB, Nair A, Merritt WM, Han LY, Armaiz-Pena GN, et al. Curcumin inhibits tumor growth and angiogenesis in ovarian carcinoma by targeting the nuclear factor-kB pathway. Clin Cancer Res 2007;13(11):3423–30.
[20] Cheng AL, Hsu CH, Lin JK, Hsu MM, Ho YF, Shen TS, et al. Phase I clinical trial of curcumin, a chemopreventive agent, in patients with high-risk or pre-malignant lesions. Anticancer Res 2001;21(4B):2895–900.
[21] Sharma RA, Euden SA, Platton SL, Cooke DN, Shafayat A, Hewitt HR, et al. Phase I clinical trial of oral curcumin: biomarkers of systemic activity and compliance. Clin Cancer Res 2004;10(20):6847–54.
[22] Anand P, Kunnumakkara AB, Newman RA, Aggarwal BB. Bioavailability of curcumin: problems and promises. Mol Pharm 2007;4(6):807–18.
[23] Dhillon N, Aggarwal BB, Newman RA, Wolff RA, Kunnumakkara AB, Abbruzzese JL, et al. Phase II trial of curcumin in patients with advanced pancreatic cancer. Clin Cancer Res 2008;14(14):4491–9.
[24] Wang Y-J, Pan M-H, Cheng A-L, Lin L-I, Ho Y-S, Hsieh C-Y, et al. Stability of curcumin in buffer solutions and characterization of its degradation products. J Pharm Biomed Anal 1997;15(12):1867–76.
[25] Huang M-T, Newmark HL, Frenkel K. Inhibitory effects of curcumin on tumorigenesis in mice. J Cell Biochem Suppl 1997;27:26–34.
[26] Liang G, Shao L, Wang Y, Zhao C, Chu Y, Xiao J, et al. Exploration and synthesis of curcumin analogues with improved structural stability both in vitro and in vivo as cytotoxic agents. Bioorg Med Chem 2009;17(6):2623–31.
[27] Youssef D, Nichols CE, Cameron TS, Balzarini J, De Clercq E, Jha A. Design, synthesis, and cytostatic activity of novel cyclic curcumin analogues. Bioorg Med Chem Lett 2007;17(20):5624–9.
[28] Li L, Ahmed B, Mehta K, Kurzrock R. Liposomal curcumin with and without oxaliplat, effects on cell growth, apoptosis, and angiogenesis in colorectal cancer. Mol Cancer Ther 2007;6(4):1276–82.
[29] Narayanan NK, Nargi D, Randolph C, Narayanan BA. Liposome encapsulation of curcumin and resveratrol in combination reduces prostate cancer incidence in PTEN knockout mice. Int J Cancer 2009;125(1):1–8.
[30] Chen C, Johnston TD, Jeon H, Gedaly R, McHugh PP, Burke TG, et al. An in vitro study of liposomal curcumin: stability, toxicity and biological activity in human lymphocytes and Epstein-Barr virus-transformed human B-cells. Int J Pharm 2009;366(1–2):133–9.
[31] Shankeshi J, Aukunuru J. Preparation, characterization and evaluation of antidiabetic activity of a liposomal formulation encapsulating curcumin, an ayurvedic natural product. Pharmacist 2008;3(2):1–5.
[32] Marczylo TH, Verschoyle RD, Cooke DN, Morazzoni P, Steward WP, Gescher AJ. Comparison of systemic availability of curcumin with that of curcumin formulated with phosphatidylcholine. Cancer Chemother Pharmacol 2007;60(2):171–7.
[33] Bisht S, Feldmann G, Soni S, Ravi R, Karikar C, Maitra A, et al. Polymeric nanoparticle-encapsulated curcumin ("nanocurcumin"): a novel strategy for human cancer therapy. J Nanobiotechnol 2007;5(3):1–18.
[34] Das RK, Kasoju N, Bora U. Encapsulation of curcumin in alginate-chitosan-pluronic composite nanoparticles for delivery to cancer cells. Nanomedicine 2010;6(1):153–60.
[35] Cartiera MS, Ferreira EC, Caputo C, Egan ME, Caplan MJ, Saltzman WM. Partial correction of cystic fibrosis defects with PLGA nanoparticles encapsulating curcumin. Mol Pharm 2010;7(1):86–93.
[36] Anand P, Nair HB, Sung B, Kunnumakkara AB, Yadav VR, Tekmal RR, et al. Design of curcumin-loaded PLGA nanoparticles formulation with enhanced cellular uptake, and increased bioactivity in vitro and superior bioavailability in vivo. Biochem Pharmacol 2010;79(3):330–8.
[37] Shi W, Dolai S, Rizk S, Hussain A, Tariq H, Averick S, et al. Synthesis of monofunctional curcumin derivatives, clicked curcumin dimer, and a PAMAM dendrimer curcumin conjugate for therapeutic applications. Org Lett 2007;9(26):5461–4.
[38] Safavy A, Raisch KP, Mantena S, Sanford LL, Sham SW, Krishna NR, et al. Design and development of water-soluble curcumin conjugates as potential anti-cancer agents. J Med Chem 2007;50(24):6284–8.
[39] Tomlinson R, Klee M, Garrett S, Heller J, Duncan R, Brocchini S. Pendent chain functionalized polyacetals that display pH-dependent degradation: a platform for the development of novel polymer therapeutics. Macromolecules 2002;35(2):473–80.
[40] Kunwar A, Barik A, Mishra B, Rathinasamy K, Pandey R, Priyadarsini KI. Quantitative cellular uptake, localization and cytotoxicity of curcumin in normal and tumor cells. Biochim Biophys Acta 2008;1780(4):673–9.
[41] Lin S-S, Huang H-P, Yang J-S, Wud J-Y, Hsai T-C, Lin C-C, et al. DNA damage and endoplasmic reticulum stress mediated curcumin-induced cell cycle arrest and apoptosis in human lung carcinoma A-549 cells through the activation caspases cascade- and mitochondrial-dependent pathway. Cancer Lett 2008;272(1):77–90.
[42] Choudhuri PST, Das T, Sa G. Curcumin selectively induces apoptosis in deregulated cyclin D1-expressed cells at G2 phase of cell cycle in a p53-dependent manner. J Biol Chem 2005;20:20059–68.
[43] Jacot JG, Wong JY. Endothelial injury induces vascular smooth muscle cell proliferation in highly localized regions of a direct contact co-culture system. Cell Biochem Biophys 2008;52(1):37–46.
[44] Fu M, Wang C, Li Z, Sakamaki T, Pestell RG. Cyclin D1: normal and abnormal functions. Endocrinology 2004;145(12):5439–47.
[45] Hengstschlager M, Braun K, Soucek T, Miloloza A, Hengstschlager-Ottnad E. Cyclin-dependent kinases at the G1-S transition of the mammalian cell cycle. Mutat Res 1999;436(1):1–9.
[46] Kopeček J, Kopeckova P, Minko T, Lu ZR, Peterson CM. Water soluble polymers in tumor targeted delivery. J Control Release 2001;74(1–3):147–58.
[47] Thistlethwaite AJ, Leeper DB, Moylan Jr D, Nerlinger RE. pH distribution in human tumors. Int J Rad Oncol Biol Phys 1985;11(9):1647–52.
[48] Reijngoud DJ, Tager JM. The permeability properties of the lysosomal membrane. Biochim Biophys Acta 1977;472(3–4):419–49.
[49] Meister A, Anderson ME. Glutathione. Ann Rev Biochem 1983;52:711–60.

[50] Dharap SS, Wang Y, Chandna P, Khandare JJ, Qiu B, Gunaseelan S, et al. Tumor-specific targeting of an anticancer drug delivery system by LHRH peptide. Proc Natl Acad Sci 2005;102(36):12962–7.
[51] Dharap SS, Chandna P, Wang Y, Khandare JJ, Qiu B, Stein S, et al. Molecular targeting of BCL2 and BCLXL proteins by synthetic BCL2 homology 3 domain peptide enhances the efficacy of chemotherapy. J Pharmacol Exp Ther 2006;316(3):992–8.
[52] Maeda H, Wu J, Sawa T, Matsumura Y, Hori K. Tumor vascular permeability and the EPR effect in macromolecular therapeutics: a review. J Contr Release 2000;65(1–2):271–84.
[53] Ireson C, Orr S, Jones DJL, Verschoyle R, Lim C-K, Luo J-L, et al. Characterization of metabolites of the chemopreventive agent curcumin in human and rat hepatocytes and in the rat in vivo, and evaluation of their ability to inhibit phorbol ester-induced prostaglandin E2 production. Cancer Res 2001;61(3):1058–64.